

Compact representations of convolutional neural networks via weight pruning and quantization

Giosuè Cataldo Marinò, Alessandro Petrini, Dario Malchiodi, Marco Frasca

Università degli Studi di Milano, Milano, Italy

E-mail: giosue.marino@studenti.unimi.it, {alessandro.petrini, dario.malchiodi, marco.frasca}@unimi.it

Abstract—The state-of-the-art performance for several real-world problems is currently reached by convolutional neural networks (CNN). Such learning models exploit recent results in the field of deep learning, typically leading to highly performing, yet very large neural networks with (at least) millions of parameters. As a result, the deployment of such models is not possible when only small amounts of RAM are available, or in general within resource-limited platforms, and strategies to compress CNNs became thus of paramount importance. In this paper we propose a novel lossless storage format for CNNs based on source coding and leveraging both weight pruning and quantization. We theoretically derive the space upper bounds for the proposed structures, showing their relationship with both sparsity and quantization levels of the weight matrices. Both compression rates and execution times have been tested against reference methods for matrix compression, and an empirical evaluation of state-of-the-art quantization schemes based on weight sharing is also discussed, to assess their impact on the performance when applied to both convolutional and fully connected layers. On four benchmarks for classification and regression problems and comparing to the baseline pre-trained uncompressed network, we achieved a reduction of space occupancy up to 0.6% on fully connected layers and 5.44% on the whole network, while performing at least as competitive as the baseline.

Index Terms—CNN compression, space-conscious data structures, weight pruning, weight quantization, weight sharing, source coding

I. INTRODUCTION

The methodology behind deep neural networks (DNNs) dates back to more than forty years ago. However, the availability of dedicated hardware (such as GPUs or TPUs) and of huge datasets recently allowed to maximize the performance of several DNN-based predictors, setting in practice the state-of-the-art for several problems of image processing, financial forecasting, and so on. Convolutional neural networks (CNNs) played a key role in this advancement, and several such pre-trained models, such as for instance AlexNet [1] and VGG16 [2], are available for use as base models for the applications of transfer learning techniques [3]. In any case, such models have a considerable memory footprint: for instance, the above mentioned VGG16 demands around 500 MB. This also impacts on the energy consumption required to query such models, thus limiting their use in mobile phones, smartwatches, and in general within the IoT world. As a matter of fact, the need of *space-conscious* models is actually emerging in several machine learning applications [4]. Although some learning approaches directly produce succinct models [5], in this paper we consider the problem of *compressing* pre-

trained CNNs, whilst not altering their structure, so as to be able to reuse the wealth of available models and their full capabilities. This is not a limitation, as other compression approaches varying the network topology can be earlier applied. Specifically, we aim at preserving the original structure of pre-trained models while suitably adjusting the representation of their parameters, as well as the way they are stored. To this end, two novel storage formats are presented here, namely *Huffman Address Map* (HAC) and *sparse Huffman Address Map* (sHAC), able to extract the knowledge distributed onto millions, or even billions, of connection weights of a learnt network, transforming it in another structure exhibiting a considerably smaller memory footprint, without sacrificing its performance (or even improving it). This is achieved by jointly applying lossy compression schemes for the NN weights and entropy coding techniques for the lossless representation of the compressed weights. Our goal to not modify the original network structure imposed to select in the vast domain of CNN compression methodologies those ensuring this property, that is weight pruning and quantization. Subsequently, the proposed representations are devised to benefit from both these two techniques, and combine entropy coding, address maps, and compressed sparse column (CSC) representations. Concerning the compression schemes, the top-performing quantization methods in literature have been considered, including a recently proposed probabilistic technique borrowed from the realm of federated learning.

We tested the proposed methodology using two publicly available CNNs and four benchmarks (two datasets for image classification and two for the prediction of drug-target affinity), obtaining as a result the confirmation that a well-conceived compression can even lead to better performance w.r.t. uncompressed models. These experiments provided important indications about the behaviour of individual compression schemes when applied to both convolutional and dense layers, with the latter yielding in average higher performance and compression rates. When applied to the whole model (hence to both types of layer simultaneously), our representations achieved compression rates up to around 20×, while not worsening the model performance.

The paper is organized as follows: Sect. II describes the principal approaches for CNN compression, while Sects. III and IV describe the considered compression and representation techniques. Section V illustrates the above mentioned experimental comparison, depicted in terms of performance gain/degradation, achieved compression rate, and execution

times. Some concluding remarks end the paper.

II. RELATED WORK

Existing DNN compression methods can be classified into five broad categories, i.e., weight pruning, weight quantization, low-rank matrix and tensor decomposition, knowledge distillation and structural compression. In this distinction, the techniques based on weight sharing are included in the broader category of weight quantization. The above mentioned categories are separately described here below. The reader interested to a thorough review of compression methods for NNs can refer for instance to [6], [7].

A. Weight pruning

Weight pruning is likely the most commonly used technique to lower the number of parameters in a DNN. It consists in eliminating connections deemed as irrelevant, thus reducing the number of parameters, while clamping the weight matrix dimension (unless in structural compression, see Sect. II-E). Libraries for sparse matrix multiplication (SM) can be used to take full advantage of the memory reduction. However, SM tends to be slower than its dense counterpart; as a consequence, structural compression is often jointly applied with pruning. The simplest pruning strategy involves to set a threshold τ and remove weights whose absolute value is lower than τ [8]. The threshold can be layer specific, or it can be set for the whole network. This criterion, often called magnitude-based pruning, involves a subsequent fine-tuning (retraining) of the remaining weights. In another class of pruning approaches, (L_1 or L_2) regularization terms drive the learning algorithm to output a network in which several weights have negligible values, so that pruning becomes a straightforward post-training step [9].

Pruning has also been performed via genetic algorithms [10] and particle swarm optimization [11]. Using these techniques, weights initially removed can be reinserted; however, their complexity allows application to DNNs of limited size.

B. Weight quantization

In neural networks, *quantization* consists in fixing the number of bits used to represent weights, activations or gradient values. This leads to a compressed model for instance when single precision floating point (FP32, as each value requires 32 bits) is used in place of standard double precision. Half-precision FP (FP16) and integer arithmetic (INT16) are also commonly considered. To reduce memory footprint, and speed up training, even smaller precisions have been recently evaluated, considering short integers (INT8, INT4, INT2), or just 1-bit [12]. In any case, using less than 32 bits can yield unacceptable performance decays. A standard approach in this context is to replace FP operations with integer ones, sometimes adding a further training ameliorating the accuracy compromise during this replacement [13]. Linear and logarithmic schemes using less than 8 bits have been applied achieving a limited accuracy drop [14]. Stochastic techniques also have a role in letting FP16-based DNNs converge to a test accuracy comparable to that of their FP32 counterparts [15]. An extreme

quantization takes place with *binarization*, in which a single bit and logic gates are used for representation and FP operations, with a strong memory reduction at the expense of an accuracy drop [16]. A hybrid approach quantizes values in narrow regions, using higher precision for the remaining values. Thus, a smaller number of bits is used for the regions in which most values lie, leading to smaller quantization errors [17]. Loss-aware strategies have also been used to contain the penalty induced by quantization. In [18] the compression scheme $\mathbf{W} = \alpha\mathbf{B}$ is adopted, where $\alpha \in \mathbb{R}$ and \mathbf{B} have binary entries, and the loss is minimized over α and \mathbf{B} . Similarly, weights are first divided in two groups, then only one group is quantized using solely powers of 2 as weights [19]. In weight sharing techniques, weights are partitioned into k categories, and a representative value replaces all weights in its category. When k is low, representatives can be stored with full precision in a vector \mathbf{r} , and keep in memory the matrix \mathbf{I} containing pointers to \mathbf{r} ; as pointers require less space than FP32 weights (e.g., INT8 when $k \leq 256$), \mathbf{I} is more compact than \mathbf{W} and largely compensates for the additional \mathbf{r} [20]. We will refer to this approach as *index map*. These methods mainly differ in the representative selection, e.g., by means of clustering [20], statistical methods [21], [22], and partitioning schemes [23], [24]. Details about these methods are given in Sect. III.

C. Low-rank matrix and tensor decomposition

DNNs can be compressed by decomposing weight tensors in a lower rank approximation: a matrix $\mathbf{W} \in \mathbb{R}^{n \times m}$ of full rank r can be decomposed as $\mathbf{W} = \mathbf{A}\mathbf{H}$, where $\mathbf{A} \in \mathbb{R}^{n \times r}$ and $\mathbf{H} \in \mathbb{R}^{r \times m}$, moving space complexity from $\mathcal{O}(nm)$ to $\mathcal{O}(r(n+m))$, with some approximation error coming from the estimate of low-rank matrices. Singular Value Decomposition (SVD) has been widely used to achieve such a decomposition [25], [26]: \mathbf{W} is factorized as $\mathbf{W} = \mathbf{U}\mathbf{\Sigma}\mathbf{V}^T$, where $\mathbf{U} \in \mathbb{R}^{n \times r}$ and $\mathbf{V} \in \mathbb{R}^{m \times r}$ are orthogonal matrices, and $\mathbf{\Sigma} \in \mathbb{R}^{r \times r}$ is the diagonal matrix of singular values. The nonzero elements of $\mathbf{\Sigma}$ are sorted in decreasing order (along with rows of \mathbf{U} and \mathbf{V}), and the top q rows are used in the approximation $\mathbf{W} \approx \mathbf{U}_q\mathbf{\Sigma}_q\mathbf{V}_q^T$, where \mathbf{X}_q is the sub-matrix containing the first q rows of \mathbf{X} . If $q < r$, it is called truncated SVD. This approach has been branched out also to tensors in recurrent NNs [27] and in CNNs [28]–[30].

D. Knowledge distillation

This compression technique encompasses different approaches to learn a ‘thinner’ DNN model, called *student*, from a larger *teacher* model, whose outputs act as soft targets for the training process. The teacher output should be a probability distribution, and the idea is to exploit the corresponding logits to ‘distill’ information to the student, which is trained minimizing the cross entropy between the teachers’ logits and its logits [31]. More precisely, the softmax layer transforms a logit z_j w.r.t. the j -th class, producing the probability q_j to be associated with that class as follows:

$$q_j := \phi(z_j) := \frac{e^{z_j/T}}{\sum_k e^{z_k/T}},$$

where $T > 1$ is a temperature parameter. Now, let v_j and z_j denote the logits of teacher and student, respectively, and

$q_j = \phi(z_j)$, $p_j = \phi(v_j)$. In [32], knowledge distillation (KD) is shown to be a special case of matching logits among two models, leading to the following cross entropy loss:

$$E(\mathbf{z}, \mathbf{v}) = - \sum_j p_j \log q_j. \quad (1)$$

The derivative of E with respect to z_j is then calculated as

$$\frac{\partial E}{\partial z_j} = \frac{1}{T}(q_j - p_j) = \frac{1}{T} \left(\frac{e^{z_j/T}}{\sum_k e^{z_k/T}} - \frac{e^{v_j/T}}{\sum_k e^{v_k/T}} \right),$$

which allows to minimize Eq. (1) and to improve the student performance exploiting the pre-trained teacher's (or ensemble of teachers) generalization ability. When distilling a linear classifier, the student is able to learn exactly the teacher's outcome if the number of examples is greater or equal to the size of the original training set. When less data is available, the student finds the best approximation of the teacher's weight vector within the subspace spanned by training data [33].

A limitation emphasized for KD is that, although the student is able to reproduce the behavior of the teacher on training data, it might lose its generalization ability. Early stopping in training the student can mitigate this drawback. Moreover, it has been discussed that the student size cannot be excessively small: a big gap between teacher and student leads to improper knowledge transmission [34]. The *teacher assistant* (TA) model, distilling an intermediate TA network from the teacher, permits to mitigate such difficulty, in the so-called *multi-step* KD. Further, label smoothing has been shown leading to performance degradation since it provides less information to the student about class boundaries [35]. Finally, a contrastive loss between teacher and student outputs has also been proposed in place of cross entropy, to preserve structural information of the embedding space [36].

E. Structural Pruning

In structural compression, inadequate components (e.g., units or layers) are pruned, usually through iterative procedures [37]. The resulting NN is faster, low power consuming, and memory-efficient, at the expense of a contained accuracy drop. Adequacy is related to the loss change incurred when a component is removed [38]. *Skeletonization*, for instance, consists in coupling each connection to an importance coefficient. The more general class of *loss sensitivity* methods calculates importance coefficients via measures of loss variation using first [39] or second order derivatives [40], and after a joint training of connections and coefficients, all units having the lowest importance coefficients are eliminated.

Dense network layers have been for instance shrunk by cutting away neurons isolated during an iterated weight pruning, adding a smaller number of new neurons to improve performance, so that the overall number of parameters monotonically decreases [41]. Analogously, filters of convolutional layers are removed in [42] when their contribution to the overall accuracy is negligible. As the number of channels in a given layer does not change across filters, the sum of the weight magnitudes can be computed as an average of weight value for each filter, pruning the latter if this average is small. An efficient approach, named ThiNet, includes in the learning objective the

rate of filters to be retained based on the output to the next layer: when this output can be accurately approximated using only a subset of its input channels, the other filters can be eliminated [43]. *Channel pruning* has also been proposed to lessen computation and storage requirements, removing unimportant channels according to their relevance in determining the layer output [44]. Finally, *layer pruning* removes some selected layers, mainly when striking compression is required (e.g., for deploying on smart devices) [45]–[47]. However, this results in higher accuracy decay due to structural deterioration of the DNN model, as some layers have specific semantics.

III. COMPRESSION TECHNIQUES

As mentioned above, in this work we focus on compressions which do not alter the structure of the pre-trained network. Therefore, the most promising state-of-the-art weight pruning and quantization techniques have been considered, with the aim to store their result via the structures proposed in Section IV (designed to leverage their compression properties). The description of such compression strategies is supplied in the following, along with some preliminary definitions.

A. Preliminary definitions

The connection weights of one layer in the network are denoted by a matrix $\mathbf{W}^o \in \mathbb{R}^{n \times m}$, whereas its compressed version is \mathbf{W} , having the same dimension of \mathbf{W}^o . Symbols w^o and w denote generic entries of \mathbf{W}^o and \mathbf{W} , respectively. The *occupancy ratio* of \mathbf{W} is defined as $\psi = \frac{\text{size}(\mathbf{W}^o)}{\text{size}(\mathbf{W})}$ (reciprocal of *compression ratio*), where $\text{size}(x)$ is the memory size of x . Boldface and italic boldface is used for matrices and vectors (e.g., \mathbf{W} and \mathbf{x}), while $|\cdot|$ is a cardinality operator returning the length of a string or the number of elements in a vector; $\mathbf{1}_A$ denotes the characteristic function of a set A . The log function always refers to the binary logarithm. Finally, $s \in [0, 1]$ is the ratio of non-zero elements in \mathbf{W} (number of non-zero entries divided by nm), and $1 - s$ its *sparsity coefficient*.

B. Weight Pruning

We implemented weight pruning (see Sect. II) removing weights that are small in absolute value. After having fixed an empirical percentile w_p of the entries of \mathbf{W}^o , we defined \mathbf{W} by setting $w = w^o$ if $|w| > w_p$, 0 otherwise. The time complexity is $\mathcal{O}(nm \log(nm))$, as the sorting step needed for the computation of w_p dominates the overall procedure. We subsequently retrained the network on the same dataset, only updating non-null weights in \mathbf{W} . The only hyper-parameter is the percentile level p , related in turn to the sparsity coefficient. (see Sect. V for a description of how hyper-parameters of all considered compression methods have been selected).

C. Quantization via weight sharing

This quantization strategy consists in reducing the space needed to store individual weights via weight sharing (WS), expressly by casting connection weights into categories and substituting all weights in a category with their representative. This allows quantization by replacing weights with their category index. In the following, the state-of-the-art approaches in this context considered for this work are briefly introduced.

1) *Clustering-based WS (CWS)*: this strategy, fixed the number k of clusters, aims at gathering similar values in \mathbf{W}° via the k -means algorithm [48], obtaining the corresponding centroids $\{c_1, \dots, c_k\}$, and subsequently replacing each weight in \mathbf{W}° with the corresponding centroid. Centroids are stored in a vector \mathbf{c} whose indices populate the index map \mathbf{II} [20]. Thus, if w_{ij}° is associated with centroid, say, c_1 , then $\pi_{ij} = 1$. Denoted by b and \bar{b} the number of bits respectively used to store one entry of \mathbf{W}° and \mathbf{II} , the occupancy ratio is given by $\frac{bnm+kb}{bnm} = \frac{\bar{b}}{b} + \frac{k}{nm}$. For instance, when $k \leq 256$, $\bar{b} = 8$, and assuming FP32 for \mathbf{W}° ($b = 32$), the occupancy would be $\simeq 1/4$. This comes at the price of two memory accesses in order to retrieve a weight. The time complexity is $\mathcal{O}(k(mn)^2)$ (due to k -means). A retraining phase is then applied, ensuring weights always assume values in the centroid set. This is achieved by using the cumulative gradient

$$\frac{\partial \mathcal{L}}{\partial c_l} = \sum_{i,j} \frac{\partial \mathcal{L}}{\partial w_{ij}} \mathbb{1}(\pi_{ij} = l),$$

where $l \in \{1, \dots, k\}$. This might end up in using less than k weights, if two or more centroids converge to a same value during retraining. To achieve a higher compression, in [20] pruning and CWS have been applied in chain, with weight sharing considering non-null weights identified by pruning.

2) *Probabilistic WS (PWS)*: this technique is based on a weight sharing technique named *Probabilistic Quantization*, recently proposed in [21] and relying on a probabilistic transformation analogous to those mapping weights onto special binary or ternary values proposed in [49], [50]. Given $\underline{w} = \min \mathbf{W}^\circ$, $\bar{w} = \max \mathbf{W}^\circ$, PWS is based on the following probabilistic rationale: suppose that each learnt weight w° is the specification of a random variable W° with support $\mathcal{W} := [\underline{w}, \bar{w}]$. If W denotes the two-valued random variable defined by $P(W = \underline{w}) = \frac{\bar{w} - w^\circ}{\bar{w} - \underline{w}}$, $P(W = \bar{w}) = \frac{w^\circ - \underline{w}}{\bar{w} - \underline{w}}$, the specifications of W approximate a weight w through an extreme form of weight sharing, now only using two representative values. It is easy to show that $\mathcal{E}(W|W^\circ = w) = w$, so that independently of the distribution of W° ,

$$\begin{aligned} \mathcal{E}(W) &= \int_{\mathcal{W}} \mathcal{E}(W|W^\circ = w) f_{W^\circ}(w) dw = \\ &= \int_{\mathcal{W}} w f_{W^\circ}(w) dw = \mathcal{E}(W^\circ). \end{aligned}$$

As a consequence, pseudorandomly extracting a specification of W° for each entry w° and building new matrix \mathbf{W} using these specifications as entries, we obtain an highly compressible *unbiased* estimator of \mathbf{W}° . The method is extendable by partitioning \mathcal{W} in $k > 2$ intervals. A generic w° would be obtained exactly as above, by referring to \bar{w} and \underline{w} as the extremes of the sub-interval containing w° . The k sub-intervals should be chosen preserving unbiasedness: some knowledge about the distribution of \mathbf{W}° would help, like in the following example.

Example 1. Assume each element of \mathbf{W}° to be distributed uniformly over \mathcal{W} , and partition the latter set in k sub-intervals evenly spaced $[p_{i*}, p_i^*]$, for $i = 1, \dots, k$, where

$$p_{i*} = \underline{w} + \frac{i-1}{k}(\bar{w} - \underline{w}), \quad p_i^* = \underline{w} + \frac{i}{k}(\bar{w} - \underline{w}).$$

Uniformity implies $f_{\mathbf{W}^\circ}(w) = \frac{1}{\bar{w} - \underline{w}} \mathbb{1}_{\mathcal{W}}(w)$, so that

$$P(\mathbf{W}^\circ \in P_i) = \int_{\underline{w}}^{\bar{w}} f_{\mathbf{W}^\circ}(w) dw = \frac{p_i^* - p_{i*}}{\bar{w} - \underline{w}} = \frac{1}{k},$$

having all sub-intervals the same length. Similarly, it can be shown that the variance of the biased estimate \mathbf{W} quadratically decreases with k and linearly increases w.r.t. $|\mathcal{W}|$.

In general, unbiasedness can be ensured by fixing the intervals' extremes as $\chi_{\frac{i}{k}}$, for $i = 0, \dots, k$, where χ_q denotes the q -quantile of \mathbf{W}° . The time and space complexity respectively amount to $\mathcal{O}(nm \log(nm))$ (due to quantile computation) and $\mathcal{O}(mn+k)$. Note that, analogously to CWS, post-compression retraining using the cumulative gradient is needed for PWS, which can also be applied in combination with pruning.

3) *Uniform Quantization (UQ)*: this quantization scheme, which selects representative weights uniformly in the weight domain, has been proven yielding an entropy asymptotically smaller than that of any other quantizer, regardless of the source statistics, under the assumption that the source has a reasonably smoothed density function [51]. Banking upon this result, in [23] UQ has been formalized so as to transform the weight w° according to the following scheme:

$$w = \delta \cdot \text{round}((w^\circ + d)/\delta) - d,$$

where $\delta > 0$ is the interval size, $d \in [-\frac{\delta}{2}, \frac{\delta}{2}]$ is a constant bias, and round is the rounding function. δ must be selected based on compression ratio and/or accuracy requirements and the number k of distinct weights desired: compression ratio increases while accuracy degrades and k decreases, as δ grows.

4) *Entropy Constrained Scalar Quantization (ECSQ)*: this compression strategy (also known as Entropy Coded Scalar Quantization) [24], [52] transforms a signal described through a random variable onto quantized values. In the realm of NN, the random variable, its specifications, and the quantized values correspond to W° , w° , and w in our notation. ECSQ partitions the domain of W° in k decision levels, each identified by an interval \mathcal{W}_i , and selects an analogous number of representation levels w_i . All values belonging to a decision level are transformed onto the corresponding representation. Decision and representation levels are chosen jointly optimizing the expected value for the quantization distortion D (using a prefixed distortion measure such as MSE) and the entropy H of the resulting distribution of representation levels. The optimal ECSQ scheme has been found minimizing distortion constraining entropy to not exceed a prefixed threshold [51], considering for instance the optimization of the Lagrange cost

$$D + \lambda H = \frac{1}{nm} \sum_{i=1}^k \sum_{j \in \mathcal{W}_i} (|w_j^\circ - w_i|^2 - \lambda \log_2 p_i),$$

where λ is a Lagrange multiplier, and $p_i = |\mathcal{W}_i|/(nm)$. ECSQ and UQ have shown the best trade-off accuracy/compression rate in a recent state-of-the-art comparison [23].

IV. COMPRESSED MATRIX REPRESENTATION

Once the techniques described in Sect. III have been applied, the resulting matrix \mathbf{W} has the same dimensions of the

original matrix. Here we first describe the classical CSC format, then the proposed compact structures to store \mathbf{W} , exploiting the sparsity and presence of repeated values.

A. Compressed sparse column

The *compressed sparse column* (CSC) format [53] is a standard for storing sparse matrices. It is composed of 3 arrays:

- \mathbf{nz} , containing the nonzero values, listed by columns;
- \mathbf{ri} , containing the row indices of elements in \mathbf{nz} ;
- \mathbf{cb} , where the difference $cb_{i+1} - cb_i$ provides the number of nonzero elements in column i ; thus, \mathbf{cb} has dimension $m + 1$, where $cb_{m+1} = cb_1 + |\mathbf{nz}|$.

Example 2. Consider the matrix

$$\mathbf{W} = \begin{pmatrix} 1 & 0 & 4 & 0 & 0 \\ 0 & 10 & 0 & 0 & 0 \\ 2 & 3 & 0 & 0 & 5 \\ 0 & 0 & 0 & 0 & 0 \\ 0 & 0 & 0 & 0 & 6 \end{pmatrix}.$$

Its CSC representation is $\mathbf{nz} = (1, 2, 10, 3, 4, 5, 6)$, $\mathbf{ri} = (1, 3, 2, 3, 1, 3, 5)$, and $\mathbf{cb} = (1, 3, 5, 6, 6, 8)$.

Let $q = |\mathbf{nz}|$ be the number of nonzero elements in \mathbf{W} , and denote henceforth by b the number of bits used to represent every element of the matrix (one memory word), so that we need bnm bits to store \mathbf{W} , and $(2q + m + 1)b$ to store its CSC representation¹. The occupancy ratio is given by $\psi_{CSC} = \frac{2q+m+1}{nm}$. Given the non-zero ratio s of \mathbf{W} , it holds $q = snm$, thus $\psi_{CSC} < 1$ implies $s < \frac{1}{2} - \frac{(m+1)}{2nm}$. The dot product $\mathbf{x}^T \mathbf{W}$ can be computed using a custom procedure for the CSC format, having a time complexity of $\mathcal{O}(q)$ [53] and which can be sped up through parallel computing. Using b bits for each matrix element constitute the main limitation of CSC, whereas better compactness and bit-memory efficiency can be achieved using variable-length coding.

B. Huffman address map compression

The idea of using Huffman coding for the representation of the weight matrix resulting from pruning and quantization has been suggested, but not realized, in [20]. In this section we provide our realization and its thorough explanation, along with its space upper bound first derived here. We call the resulting technique *Huffman Address Map compression* (HAC), as it is based on Huffman coding and address map logic; we remark that this technique applies a lossless compression, as well as in CSC. Address maps organize the matrix entries as a row- or column-order based sequence of bits, in which 0 identifies any null entry, while each remaining element z is represented by a binary string $a(z)$ encoding its address.

Example 3. The bit sequence corresponding to the column-order based address map for the matrix \mathbf{W} of Example 2 is

$$a(1)0a(2)000a(10)a(3)00a(4)00000000000a(5)0a(6) .$$

¹we assumed b bits also for the components of \mathbf{ri} , although they can be represented using only $\lceil \log n \rceil$ bits, which might be lower than b .

Of course, in order to achieve efficiency it is necessary to rely on compact representations for addresses. We implemented $a(z)$ via the corresponding Huffman coding $H_{\mathbf{W}}(z)$, in view of its well-known properties: it is instantaneous, uniquely decodable and it has a near-optimal compression rate [54]. More precisely, if we consider a source (w_1, \dots, w_l) , the corresponding probabilities (p_1, \dots, p_l) , and denote

- by $\mathcal{H} = -\sum_{i=1}^l p_i \log p_i$ the source entropy, which by Shannon's source coding theorem corresponds to the minimal average number of bits per symbol [55], and
- by $\bar{H}_{\mathbf{W}} := \sum_{i=1}^l p_i |H_{\mathbf{W}}(w_i)|$ the average number of bits per symbol attained when using the Huffman coding,

it can be shown that $\mathcal{H} \leq |\bar{H}_{\mathbf{W}}| \leq \mathcal{H} + 1$.

To get uniquely decodable strings we also include zeroes in the Huffman code. This brings us to a total of $q+1$ codewords. We denote by $\text{HAC}(\mathbf{W})$ the bit stream encoding \mathbf{W} , and split the former into $N = \lceil |\text{HAC}(\mathbf{W})|/b \rceil$ memory words, in turn denoted as $\text{HAC}(\mathbf{W})_1, \dots, \text{HAC}(\mathbf{W})_N$ and represented as an array $\mathcal{C}_{\text{HAC}}(\mathbf{W})$ of N unsigned integers. Zero-padding is added to the last word when $|\text{HAC}(\mathbf{W})|$ is not a multiple of b .

Fact 1. (HAC worst case) If \mathbf{W} is dense and it does not contain repeated entries,

$$|\text{HAC}(\mathbf{W})| \leq nm(1 + \log(nm)) + 6nmb$$

when B-trees are used to represent both dictionaries implementing the mappings $H_{\mathbf{W}}$ and $H_{\mathbf{W}}^{-1}$.

Proof. By hypothesis each of the nm symbols of \mathbf{W} appear exactly once, thus $\mathcal{H} = \log(nm)$, the corresponding Huffman code $H_{\mathbf{W}}$ has an average codeword length upper-bounded by $1 + \log(nm)$ and at most $nm(1 + \log(nm))$ bits are needed. Assuming each value in the B-tree is represented trough 1 word (b bits), each dictionary requires $3b$ bits per entry: $2b$ bits to store each pair $(z, H_{\mathbf{W}}(z))$, and at most b bits to store a pointer in the B-tree structure (this is overestimated since we have less pointers than keys in a B-tree). The thesis follows. \square

The upper bound provided by Fact 1 can be reduced, as there are methods storing a n -symbols Huffman code using at most $\lceil 10.75n \rceil - 3$ bits [56]. Moreover, $nm(1 + \log(nm)) + 6nmb$ is larger than the number of bits required by an uncompressed matrix. For this reason, alternative representations should be used when the matrix is dense and no assumptions can be made on the weight distribution. On the other hand, in the next corollary we show that the HAC becomes convenient when a relatively small number k of distinct values are contained in \mathbf{W} , as customary with quantized matrices (see Sect. III).

Corollary 1. If \mathbf{W} is dense and composed of $k < nm$ distinct values,

$$|\text{HAC}(\mathbf{W})| \leq nm(1 + \log k) + 6kb.$$

Proof. In the worst case, all symbols are equally probable, the source entropy is $\mathcal{H} = \log k$, so that to represent the nm values $nm(1 + \log(k)) + 6kb$ are required at most, including the overhead due to the dictionaries for the k codewords. \square

Corollary 1 leads to the following upper bound:

$$\psi_{\text{HAC}} \leq \frac{1 + \log k}{b} + \frac{6k}{nm} \quad (2)$$

with reference to the uncompressed matrix, where, as expected, for small k the first term is more relevant, while the second term grows faster with k .

Algorithm 1 Dot procedure for HAC representation.

Procedure Dot_{HAC}

Input: compressed array $\mathcal{C}_{\text{HAC}}(\mathbf{W})$; decoding dictionary $H_{\mathbf{W}}^{-1}$; vector $\mathbf{x} \in \mathbb{R}^{n \times 1}$; number of compressed words N ;

begin algorithm

```

1: Initialize:  $out := \text{zeros}(n)$ ,  $row := 1$ ,  $col := 1$ 
                $sum := 0$ ,  $rem := null$ ,  $oset := 0$ 
2: for  $i = 1$  to  $N$  do
3:    $S := \text{getBinarySeq}(\mathcal{C}_{\text{HAC}}(\mathbf{W})[i])$ 
4:   while  $[oset, rem, z] := \text{NCW}(S, rem, oset) \neq null$  do
5:      $sum := sum + x[row] * H_{\mathbf{W}}^{-1}(z)$ ,  $row := row + 1$ 
6:     if  $row > n$  then
7:        $row := 1$ ,  $out[col] := sum$ 
8:        $col := col + 1$ ,  $sum := 0$ 
9:     end if
10:  end while
11: end for

```

end algorithm

Output: out , that is $\mathbf{x}^T \mathbf{W}$.

Dot product. The procedure Dot_{HAC} (Algorithm 1) shows how the dot product $\mathbf{x}^T \mathbf{W}$ can be computed when \mathbf{W} is represented through HAC. Each compressed word in $\mathcal{C}_{\text{HAC}}(\mathbf{W})$ is processed sequentially, obtaining its binary representation S (line 3), which is scanned in a loop (lines 4-10) to retrieve code words. The procedure NCW gets the next code word from S , considering an offset $oset$ and possibly adding unprocessed bits from the previous word (stored in rem). NCW returns $null$ when it is not possible to detect a code word. This means that it took two adjacent memory words to represent the next code word. When this happens, rem is updated accordingly and the processing considers the next word at the successive iteration (line 2). Zero-padding is also handled by the procedure. Subsequently, the weight for the detected code word is computed and multiplied by the corresponding element in \mathbf{x} , and accumulated in sum (line 5). Thus only one weight at a time is kept in main memory. The time complexity of the external N iterations is $\mathcal{O}(|\mathcal{C}_{\text{HAC}}(\mathbf{W})|) = \mathcal{O}(Nb)$ (line 3), amounting in worst case (uniform frequencies of distinct weights) to $\mathcal{O}(nm \log k)$. Moreover, time complexity for lines 5-8 is $\mathcal{O}(N)$, and that of executions of line 4 is $\mathcal{O}(Nb \log k)$. Here we assume that

- each time a bit is read from S , the current string is searched for in the dictionary (and in the worst case we need to entirely scan S), and
- searching in a dictionary of k entries can be performed in $\mathcal{O}(\log k)$ time.

Summing up, the overall time complexity is $\mathcal{O}(nm \log k)$. In Sect. IV-D we describe how the procedure Dot_{HAC} can be reworked in order to speed up the computations.

C. Sparse Huffman address map compression

HAC marginally benefits from sparsity: indeed, in such a case the space occupancy is only indirectly reduced, because now the symbol 0 has higher frequency and the Huffman code is more compact. But when \mathbf{W} is sparse and very large, we would use in any case a high amount of memory (e.g., $10(1-s)$ GB for a $10^5 \times 10^5$ matrix). To address this issue, we propose to extend HAC into the novel *sparse Huffman Address Map compression* (sHAC), in which the bit stream and the Huffman code are computed excluding the symbol 0. More precisely, \mathbf{W} is represented using a bitwise CSC format, obtaining $\mathbf{nz}, \mathbf{ri}, \mathbf{cb}$ as in Sect. IV-A: the first vector is stored using HAC, the others are kept uncompressed. The Huffman code $H_{\mathbf{nz}}$ for non-null elements is computed, obtaining by concatenation the bit stream $\text{HAC}(\mathbf{nz}) = H_{\mathbf{nz}}(nz_1) \dots H_{\mathbf{nz}}(nz_q)$, which is stored in the array $\mathcal{C}_{\text{HAC}}(\mathbf{nz})$ of $N_1 = \lceil |\text{HAC}(\mathbf{nz})|/b \rceil$ memory words. Finally, we build the sHAC representation of \mathbf{W} , denoted by $\text{sHAC}(\mathbf{W})$, as the sequence of vectors $\mathcal{C}_{\text{HAC}}(\mathbf{nz}), \mathbf{ri}, \mathbf{cb}$. The following fact establishes an upper bound for $|\text{sHAC}(\mathbf{W})|$.

Fact 2. (*sHAC worst case*) If \mathbf{W} contains snm non-null elements, with $s \in [0, 1]$ the ratio of non-zero entries in \mathbf{W} ,

$$|\text{sHAC}(\mathbf{W})| \leq snm(1 + \log(snm)) + b(7snm + m + 1)$$

when B-trees are used to represent both dictionaries implementing the mappings $H_{\mathbf{nz}}$ and $H_{\mathbf{nz}}^{-1}$.

Proof. In the worst case, all snm symbols are distinct, $\mathcal{H} = \log(snm)$, and the average codeword length of $H_{\mathbf{nz}}$ is upper bounded by $1 + \log(snm)$, thus

$$|\mathcal{C}_{\text{HAC}}(\mathbf{nz})| \leq snm(1 + \log snm).$$

The dictionaries $H_{\mathbf{nz}}, H_{\mathbf{nz}}^{-1}$ require $6snmb$ bits, vectors \mathbf{ri}, \mathbf{cb} require $b(snm + m + 1)$ bits, and the thesis follows. \square

From Fact 2 the occupancy ratio for sHAC is such that

$$\psi_{\text{sHAC}} \leq \frac{s(1 + \log snm)}{b} + 7s + \frac{m + 1}{nm},$$

and using the same argumentations given for HAC, we can show that also sHAC benefits from the matrix quantization.

Corollary 2. In the same hypotheses of Fact 2, if \mathbf{W} contains $k < nm$ distinct values,

$$|\text{sHAC}(\mathbf{W})| \leq snm(1 + \log k) + b(6k + snm + m + 1).$$

Proof. As in Corollary 1, $\mathcal{H} = \log k$, and the snm values can be represented using at most $snm(1 + \log k)$ bits. The result follows because $6kb$ bits are needed by the dictionaries for the k codewords, and \mathbf{ri} and \mathbf{cb} require $b(snm + m + 1)$ bits. \square

The occupancy ratio for sHAC is in this case such that

$$\psi_{\text{sHAC}} \leq \frac{s(1 + \log k)}{b} + \frac{6k + m + 1}{nm} + s, \quad (3)$$

where the ratio of non-zero entries s appears as last term, as well as in the first one, where it is scaled by the upper bound of ψ_{HAC} , emphasizing a gain when the sparsity of \mathbf{W} increases.

Algorithm 2 Dot procedure for sHAC representation.

Procedure Dot_{sHAC}

Input: compressed array $C_{\text{sHAC}}(\mathbf{nz})$; row index vector \mathbf{ri} ; vector \mathbf{cb} ; vector $\mathbf{x} \in \mathbb{R}^{n \times 1}$; decoding dictionary $H_{\mathbf{nz}}^{-1}$; number of compressed words N_1 ;

begin algorithm

```

1: Initialize:  $out := \text{zeros}(n)$ ,  $pos := 1$ ,  $col := 1$ 
                $sum := 0$ ,  $rem := null$ ,  $oset := 0$ 
2: for  $i = 1$  to  $N_1$  do
3:    $S := \text{getBinarySeq}(C_{\text{sHAC}}(\mathbf{nz})[i])$ 
4:   while  $[rem, oset, z] := \text{NCW}(S, rem, oset) \neq null$  do
5:     while  $cb[col + 1] = pos$  do
6:        $col := col + 1$ ,  $out[col] := 0$ 
7:     end while
8:      $sum := sum + x[ri[pos]] * H_{\mathbf{nz}}^{-1}(z)$ ,  $pos := pos + 1$ 
9:     if  $cb[col + 1] = pos$  then
10:       $out[col] := sum$ 
11:       $sum := 0$ ,  $col := col + 1$ 
12:     end if
13:   end while
14: end for

```

end algorithm

Output: out , that is $\mathbf{x}^T \mathbf{W}$.

From Eqs.(2) and (3) it follows $\psi_{\text{sHAC}} < \psi_{\text{HAC}}$ when

$$s < \frac{\frac{1+\log k}{b} - \frac{m+1}{nm}}{1 + \frac{1+\log k}{b}}.$$

Dot product. Algorithm 2 shows the dot product $\mathbf{x}^T \mathbf{W}$ when \mathbf{W} is represented through sHAC. The compressed words of $C_{\text{sHAC}}(\mathbf{nz})$ are extracted sequentially, computing each time their binary representation (line 3) and detecting code words (lines 4–13). Here, NCW is the same procedure as in Dot_{HAC}, whereas the loop at lines 5–7 possibly skips empty columns. The variable pos contains the position of the current element in \mathbf{nz} . The weight for the detected codeword is computed in line 8 and multiplied by the corresponding element in \mathbf{x} , finally updating the cumulative value contained in sum . The required time complexity is (i) $\mathcal{O}(N_1 b) = \mathcal{O}(snm \log k)$ for the N_1 iterations in the external loop (line 3), (ii) $\mathcal{O}(snm \log k)$ for line 4, (iii) $\mathcal{O}(m)$ for the loop in lines 5–7, (iv) $\mathcal{O}(N_1)$ for lines 8–12. Summing up, the overall time complexity is $\mathcal{O}(snm \log k)$. The following subsection describes how to speed up the Dot_{HAC} and Dot_{sHAC} procedures.

D. Speeding up the dot product of HAC and sHAC

The procedures Dot_{HAC} and Dot_{sHAC} can be adapted to parallel computation by exploiting the parallel nature of matrix multiplication, since any row of the left operand can undergo independently of the other rows to the dot product with the columns of the other operand. Indeed, given two matrices \mathbf{X} and \mathbf{W} , with \mathbf{W} compressed with either HAC or sHAC, the evaluation of $\mathbf{X}^T \mathbf{W}$ can be distributed across q computing units by considering q chunks of rows of \mathbf{X} , performing q dot products $\mathbf{X}_i^T \mathbf{W}$, $i \in \{1, \dots, q\}$, and finally aggregating the output matrix. \mathbf{X}_i here denotes the submatrix composed of

the rows of \mathbf{X} in the i -th chunk. By definition, there is no data dependency between each product $\mathbf{X}_i^T \mathbf{W}$, hence each chunk can be evaluated concurrently. The pseudo-code of the procedure is shown in Algorithm 3. Line 2 computes the row indices of the matrix to be assigned to each computing unit hence Idx contains q tuples. In lines 3–9 each computing unit (concurrently) contributes to k lines of out (except for the last one if n is not a multiple of q) by, in total, evaluating $k \times t$ dot products, given t the number of (encoded) columns of \mathbf{W} .

Algorithm 3 Pseudocode of the parallel matrix multiplication for HAC representation.

Procedure ParDot_{HAC}

Input: compressed array $C_{\text{HAC}}(\mathbf{W})$; decoding dictionary $H_{\mathbf{W}}^{-1}$; expanded matrix $\mathbf{X} \in \mathbb{R}^{n \times m}$; number of compressed words N ; number of computing units q ;

begin algorithm

```

1: Initialize:  $out := \text{zeros}(n, t)$ ;  $k := \lceil \frac{n}{q} \rceil$ 
2:  $Idx = [(1, k), (k+1, 2k), \dots, (k(q-1)+1, n)]$ 
3: for  $(startIdx, endIdx)$  in  $Idx$  in parallel do
4:   for  $i = startIdx$  to  $endIdx$  do
5:      $\mathbf{x} = \mathbf{X}[i, :]$ 
6:      $y_i = \text{Dot}_{\text{HAC}}(C_{\text{HAC}}(\mathbf{W}), H_{\mathbf{W}}^{-1}, \mathbf{x}, N)$ 
7:      $out[i, :] = y_i$ 
8:   end for
9: end for

```

end algorithm

Output: out , that is $\mathbf{X}^T \mathbf{W}$.

Note that the analogous parallel version for sHAC can be derived by adding as inputs $C_{\text{sHAC}}(\mathbf{nz})$, the row index vector \mathbf{ri} and the vector \mathbf{cb} , and by invoking in line 6 $y_i = \text{Dot}_{\text{sHAC}}(C_{\text{sHAC}}(\mathbf{W}), \mathbf{ri}, \mathbf{cb}, H_{\mathbf{W}}^{-1}, \mathbf{x}, N)$. To test the viability of this approach, we implemented this strategy by means of CPU multi-threading. However, the Python global interpreter lock poses severe limitations to multi-threaded execution. To overcome this limitation, ParDot_{HAC} has been implemented in C++, which provides no limitations to multi-threading, while the rest of the code is executed within Python, using the Pybind11² library for Python / C++ interoperability.

V. EXPERIMENTS AND RESULTS

In this section we empirically compare the illustrated techniques. The experiments considered four datasets and two uncompressed neural networks, as detailed here below.

A. Data

- *Classification.* MNIST [57], a benchmark of handwritten digits, containing a train set of 60K 28x28 grayscale images and a test set of 10K analogous images; CIFAR-10 [58], a dataset of 50K (train set) + 10K (test set) 32x32 color images. Both datasets refer to ten classes (one for each digit) and their labels are balanced.
- *Regression.* DAVIS [59] and KIBA [60], datasets containing the evaluation of the affinity between drugs (ligands)

²Available at: <https://github.com/pybind/pybind11>

and targets (proteins), respectively represented using the amino acid sequence and the SMILES (Simplified Molecular Input Line Entry System) string encoding. DAVIS and KIBA contain, respectively, 442 and 229 proteins, 68 and 2111 ligands, 30056 and 118254 total interactions between them, with $\frac{1}{6}$ of the data composing the test set.

B. Benchmark models

We used to publicly available pre-trained, top-performing CNN models: (i) *VGG19* [2], consisting of 16 convolutional layers followed by a fully-connected (FC) block, in turn containing two hidden layers of 4096 neurons each, and a softmax output layer³, trained on CIFAR-10 and MNIST datasets; (ii) *DeepDTA* [61], having two separate blocks for proteins and ligands, both containing three convolutional layers followed by a max pool layer and merged in a FC block consisting of three hidden layers respectively containing 1024, 1024, 512 units, and a single-neuron output layer⁴. Using pre-trained networks allows a fair analysis of compression and storage techniques, without introducing potential biases in the model selection and training procedures. Moreover, when fine-tuning weights after quantization, we preserved the same training configuration set up by the model proponents in their original work.

C. Evaluation metrics

We performed comparisons focusing on the following metrics: 1) *Accuracy* for classification and *MSE* for regression (as in original papers) or the *difference* Δ_{perf} between performances of compressed and uncompressed models; 2) ratio *time* between evaluation times of uncompressed and compressed model, and 3) occupancy ratio ψ (cfr. Sect. IV-A). When only partly compressing the NN, time and space performance only account for the actually compressed layers. The rest of the paper assesses the effectiveness of compression techniques in three scenarios, namely compressing: 1) only FC layers, 2) only convolutional layers, and 3) both layer types.

D. Software implementation

The code retrieved for baseline NNs was implemented in Python 3, using Tensorflow and Keras. We used the same environment for implementing compression and retraining (although the parallel dot procedures are written in C++). The software is distributed as a standalone Python 3 package⁵.

E. Results

We conducted multiple evaluations, analyzing the proposed compression and storage methodologies from different points of view, as described in the following dedicated subsections.

F. Preliminary results from previous studies

In this subsection we summarize the results obtained when only compressing FC layers via CWS and PWS, separately considering each layer [21].

³<https://github.com/BIGBALLON/cifar-10-cnn>.

⁴<https://github.com/hkmztrk/DeepDTA>.

⁵Source code, datasets and trained baseline networks are available at <https://github.com/AnacletoLAB/sHAM>.

TABLE I
TESTING PERFORMANCE OF ORIGINAL NON-COMPRESSED MODELS.
Performance SHOWS ACCURACY FOR MNIST/CIFAR-10 AND MSE FOR KIBA/DAVIS. *Time* IS THE OVERALL TESTING TIME.

Net	Dataset	Performance	Time (s)
VGG	MNIST	0.9954	0.888
	CIFAR-10	0.9344	0.897
DeepDTA	KIBA	0.1756	0.175
	DAVIS	0.3223	0.040

a) *Compression techniques setup*: the schemes corresponding to pruning (Pr), CWS, PWS, Pr-CWS, Pr-PWS have been tested on data and models described in Sects. V-A and V-B using the hyperparameter tuning described here below.

- *Pruning*. The percentile level p was chosen in the set $\{30, 40, 50, 60, 70, 80, 90, 95, 96, 97, 98, 99\}$;
- *CWS*. The number k of representatives for VGG19 was selected in $\{2, 32, 128, 1024\}$ for the first two FC layers of and between 2 and 32 for the (smaller) output layer; as DeepDTA is more compact, we set $k \in \{2, 32, 128\}$ in the three FC layers and $k \in \{2, 32\}$ for the output layer.
- *PWS*. To have a fair comparison, k was set as in CWS.
- *Pr-X*. The combined application of pruning followed by the quantization $X \in \{\text{CWS}, \text{PWS}\}$ was tested in two variants: a) selection of best p in terms of Δ_{perf} , and then tuning of X as in previous points; b) the vice-versa.

b) *Fine-tuning of compressed weights*: post-compression retraining was done using the same configuration as in original training. Data-based tuning was applied only to learning rate ($3 \cdot 10^{-4}$ for pruning, 10^{-3} and 10^{-4} for PWS, CWS, and combined schemes), and maximum number of epochs, set to 100. As explained in Sect. IV-B, in the experiments using only pruning the CSC representation is adopted.

c) *Performance assessment*: Table I reports the testing performance of uncompressed models as a baseline. The top performance for each compression technique, and its configuration, is shown in Supplementary Table S1, whereas the configuration improving the baseline (when existing) having the smallest memory requirement is shown in Supplementary Table S2. WQ performed better than pruning for classification, with PWS and CWS having the top performance on MNIST and CIFAR-10, respectively. Remarkably, all techniques outperformed the baseline, while exhibiting effective compression rates. Regression behaved similarly, however here pruning was preferable, and PWS never improved the baseline on KIBA. Improvements were particularly interesting on DAVIS (up to around 30% of baseline). The largest compression rate (preserving accuracy) was achieved on the biggest net, VGG19, attaining more than $150\times$ on CIFAR-10 (Pr/PWS-b and sHAC). When applied to DeepDTA, Pr/PWS-a improved the baseline MSE of 17.1%, while compressing around $18\times$.

A summary of space occupancy, time ratio, and testing performance for all used hyper-parameter configurations is shown in Supplementary Fig. S1, where sHAC is used, except for techniques producing denser matrices, where HAC was more

⁶levels smaller than 50, although not guaranteeing occupancy < 1 , were included because potentially useful in the combinations Pr-CWS and Pr-PWS.

convenient. The time reported is relative to the sequential dot procedure for HAC and sHAC. CWS and PWS combinations are reported in increasing order: first the ones with $k = 2$ in the first layer (label 2), then those with $k = 32$ in the first layer (label 32) and so on. On CIFAR-10 and DAVIS, most compression techniques outperformed the baseline, and this was likely due to overfitting, since on training data they show similar results. On MNIST and KIBA, although the baseline was only seldom improved, the compressed model used much less parameters, confirming the trend obtained in [20]. Binary quantization ($k = 2$) achieved the lowest ψ , yet a worse performance, whereas already with $k = 32$ the baseline was improved on almost all datasets. sHAC occupancy, as expected, decreased inversely with p , along with the time ratio, approaching in turn to 1 (same testing time). The high time ratios, for some configurations, reflected the fact that the dot procedure was slower than the *Numpy* dot used by baseline and leveraging parallel computation.

As pointed out in [21], these results did not highlight a compression technique better than the remaining ones. Weight pruning seemed to be preferable for regression, whereas quantization performed better in the classification setting. Overall, the most remarkable achievement can be considered the fact that compression techniques providing the lowest occupancy, i.e., those combining weight pruning and quantization, still achieved competitive or better performance than the baseline.

G. State-of-the-art comparison of HAC and sHAC

In order to assess the efficacy of the proposed formats, a suite of state-of-the-art matrix compression methods has been considered; such methods allow the execution of linear algebra operations, such as matrix-vector multiplication, directly on the compressed representation. The comparison takes into account both space reduction and multiplication time on the compressed format, and includes the following methods:

- *Compressed Linear Algebra* (CLA), a compendium of effective column compression schemes, cache-conscious operations, and a sampling-based compression algorithm to select the compression scheme more suitable for each column or group of columns; this approach achieves performance close to the uncompressed case and compression ratios similar to heavyweight formats such as Gzip, but better than lightweight formats like Snappy [62];
- three baseline formats: CSC (cfr. Sect. IV-A), *Compressed Sparse Row Format* (CSR), analogous to CSC but storing the column indices of nonzero values, instead of their rows [63], and *Coordinate list* (COO), storing non zero elements along with their row and column indices;
- *index map* (IM) [20] (see Sect. III-C1), proposed expressly in the context of neural network compression.

As baseline reference for time, we also evaluated the dot function of the *Numpy* library, which is also used by the dot product of the IM method, along with the additional access time to the vector of full precision weights. CLA is implemented in Java, and the code is available upon request from the authors. CSC, CSR and COO implementations are taken from the *Scipy* library. HAC and sHAC dot is called

within Python, but its underlying implementation is done in C++ (cfr. Sects IV-B and IV-C). The test is performed by calculating the dot product between a sparse matrix and a dense vector, without expanding the matrix. For this reason, we excluded from this evaluation other compression techniques that needed to expand the matrix to perform fine-tuning after quantizing, such as the *Tensorflow Lite Converter*⁷.

The evaluation involves the weight matrices of the three FC layers composing VGG19, trained on CIFAR-10 and MNIST, after such layers underwent pruning (various levels, from 60% to 99%) and CWS with $k = 32$ and 256 (as examples of less and more marked quantization)—as in average CWS tends to perform better than PWS on this data, as shown in Sect. V-F). Lower pruning rates were meaningless, since we are evaluating compression for sparse matrices. The dimensions of matrices for the three FC layers are 512×4096 , 4096×4096 and 4096×10 . The resulting size is the sum of the memory footprint of all involved structures (vectors, lists, dictionaries, etc.).

Comparison of the dot product performance was done generating 8 dense vectors according to a uniform distribution in $[0, 1]$, and executing the operation using as arguments each generated vector and the compressed matrix. The overall time is the sum of the 8×3 dots (8 dot products for each matrix). Executions were multi-threaded (8 threads per dot product).

Results are summarized on the graphs of Fig. 1 for $k = 32$ and in Fig. S2 for $k = 256$. Time is measured in seconds, size in Kilobytes. On both datasets, with lower pruning ($p \in [60, 90]$) and $k = 32$, HAC shows the highest compression rate, from $\simeq 21 \times$ ($p = 60$) to $\simeq 50 \times$ ($p = 90$), whereas when the matrices get highly sparse ($p \geq 90$), sHAC compresses the most—till around $361 \times$ ($p = 99$). IM, using 1 byte for each entry of the matrix when $k = 32$, has better compression ratios than CLA and sHAC only up to $p = 70$. This is reasonable, since this method does not exploit the matrix sparsity (0 is just one of the k values to be stored). CSC, CSR and COO behave in a similar way, and always occupy more than CLA and HAC/sHAC, and less than IM only when $p \geq 0.95$. On the other hand, such formats allow the fastest dot product (even faster than *Numpy* when $p > 90$), as *Scipy* is designed to perform dot products very efficiently. Among the remaining methods, with high pruning ($p > 90$) HAC and sHAC are faster than the other methods (except for *Numpy* dot). Below that boundary, IM is faster than CLA for $p \leq 70$. *Numpy* often performs the fastest dot product, but it is useless since it operates on the uncompressed matrix. Analogous trends are verified for $k = 256$, with index map that compares little more favourably, since its space and time are almost the same (it still uses only 1 Byte for entries of \mathbf{II}), while the other methods slightly increase both their space and time requirements.

Summing up, HAC and sHAC compress the most (HAC for $p \leq 90$, sHAC in the other cases), and sHAC is the best in time for $p \geq 95$ (it is still faster than the *Numpy* dot on the MNIST— $p = 99$ case). For low/medium pruning rates, IM and CLA exhibit a higher time efficiency than HAC and sHAC; these features are well expected, as our methods have been developed and optimized for obtaining state-of-the-art

⁷<https://www.tensorflow.org/lite/convert>

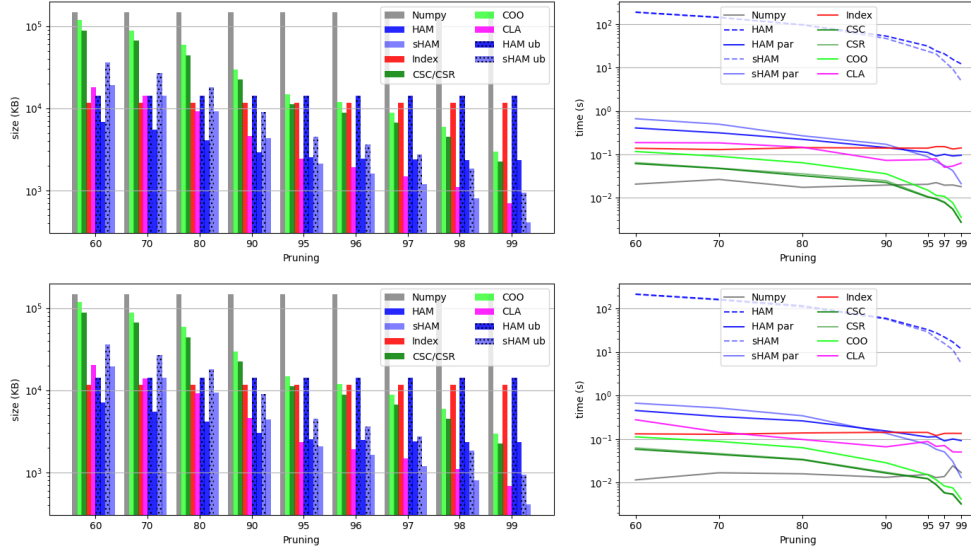


Fig. 1. Average execution times in seconds (graphs on the right) for performing 8 vector matrix product, and memory footprint in KiloBytes (graphs on the left) for storing the compressed representation of the three fully connected layer weight matrices of the VGG19 model. Top rows refer to the model trained on CIFAR-10 dataset, bottom row on MNIST dataset. All matrices were subjected to different degrees of pruning and were quantized by weight sharing (CWS) with 32 values. Dotted bars represent the upper bound of HAC and sHAC sizes evaluated with Corollaries 1 and 2. Times are reported in logarithmic scale.

compression ratios when pruning and quantization is applied, at the cost of requiring a quite consistent pruning to show fast dot products. Between IM and CLA, the former is preferable for low pruning rates in terms of both time and space.

Both figures also show the upper bounds introduced in Sects IV-B and IV-C, evaluated using Corollaries 1 and 2. Both techniques show an actual size consistently lower than the upper bound: on average, sHAC is twice as lower, while HAC ranges from $2\times$ to $6\times$ lower, depending on pruning ratio. So, the assumption of weights having the same frequency (used to compute upper bounds) is farther from being realistic, and in practice the proposed formats are definitely more effective. Tighter bounds might be found if more realistic assumptions are considered, which could be the subject of future studies.

H. Evaluation of global and per-layer quantization

The assessment performed in Sect. V-F made use of a *non-unified* quantization, selecting a specific k per layer and quantizing layers separately. In essence, all weight matrices could be quantized at the same time using a unique value of k , leading to a variant that we name *unified* quantization. Here we compare these two approaches. To this end, the setting used in Sect. V-F is preserved, that is compressing only dense layers and measuring performance in terms of accuracy/MSE and occupancy ratio. It is worth noting that the non-unified case has higher flexibility, counterbalanced by an increase of memory overhead, as each layer requires its own dictionaries. On the other hand, the unified case entails only one dictionary but the choice of k represents an ‘one size fits all’ solution, which reduces versatility and might impact on performance.

First, the best models in terms of prediction performance from Supplementary Table S1 have been considered, meanwhile using the same compression techniques. The value for k

TABLE II
COMPARISON BETWEEN UNIFIED AND NON-UNIFIED QUANTIZATION. ψ REFERS TO HAC FORMAT. BASELINE PERFORMANCE IN BRACKETS.

Net-Dataset	Type	Config	Perf	ψ
VGG19-MNIST (0.9954)	CWS	128-32-32	0.9957	0.3210
	uCWS	192	0.9957	0.2344
	PWS	32-32-2	0.9958	0.3090
	uPWS	66	0.9955	0.1857
VGG19-CIFAR-10 (0.9344)	CWS	32-32-2	0.9371	0.3060
	uCWS	66	0.9370	0.1856
	PWS	32-2-32	0.9363	0.0910
	uPWS	66	0.9366	0.1857
DeepDTA-KIBA (0.1756)	CWS	128-128-32-2	0.1679	0.3900
	uCWS	290	0.1609	0.2516
	PWS	32-128-128-32	0.1761	0.4250
	uPWS	320	0.1631	0.2642
DeepDTA-DAVIS (0.3223)	CWS	128-2-128-2	0.2320	0.2120
	uCWS	260	0.2291	0.2496
	PWS	128-32-32-32	0.2430	0.3240
	uPWS	224	0.2253	0.2469

in the unified case was selected by summing the values of k in the layers of the selected models in the non-unified case. The resulting four experiments are summarized in Table II, where the modalities exploiting the unified choice of k are marked as ‘uCWS’ and ‘uPWS’. The results point up that such variants tend to compress more than their non-unified counterparts, having in some cases negligible performance decay (classification), or even improvements (regression). Specifically, uCWS compresses up to $1.64\times$ more than CWS (VGG19-CIFAR-10), and uPWS up to $1.66\times$ more than PWS (VGG19-MNIST), while almost preserving the accuracy (-0.03% and -0.01% , respectively). Besides, uCWS improves the MSE up to 4% on DeepDTA-KIBA (while compressing $1.55\times$ more), and uPWS up to the 8% on DeepDTA-DAVIS, even with a compression ratio of $1.31\times$ higher. Nevertheless, the

above mentioned flexibility of non-unified variants let them compress more than the unified counterparts, mainly when they can use lower k values in large layers. For instance, PWS has less than half occupancy compared to uPWS on VGG19-CIFAR-10 by using only two distinct weights for the central hidden layer of VGG19 (the largest one). In order to confirm these observations, we repeated this experiment using the non-unified models reported in Supplementary Table S2 (best compression preserving the baseline performance), as shown in Supplementary Table S3. The trend of Table II is preserved, although here the higher flexibility for non-unified methods is more marked (indeed they always compress more on classification). For this reason and to better evaluate the behavior of unified versions, we additionally tested them by varying $k \in \{2^i | 1 \leq i \leq 7\}$, and reporting the setting achieving the best compression ratio among those performing at least as good as the non-unified counterparts. With this “non-constrained” setting, they show in most cases an occupancy much lower than the non-unified variants (e.g., $4\times$ smaller on VGG19-MNIST data). Notwithstanding, even in this case, the non-unified variants can sometimes have a better compression (like on VGG19-MNIST data for the CWS method).

Overall, although both variants can be better than the corresponding counterparts in some specific cases, unified approaches tend to achieve both better compression and higher performance; thus, hereafter this variant will be used.

I. Comparison of quantization techniques

As unified quantization is preferable, it has been applied to compare also the two quantization strategies described in Sect. III-C, namely UQ and ECSQ (uUQ and uECSQ for the unified version). The setting used up to now (compressing only FC layers and measuring accuracy/MSE and occupancy ratio) has been maintained. All methods have been evaluated by varying k in $\{2, 16, 32, 64, 128, 256\}$. HAC was used to store the compressed matrices, since it has proven to be more effective in this setting. Parameters λ (uECSQ) and δ (uUQ) have been tuned to give in output the number k of desired clusters, whereas to reduce the already massive set of experiments, we have set $d = 0$ for uUQ. Results are summarized in Tables III and S4. In classification, we notice that the predicting performance of all models is often comparable with the baseline, with rare exceptions in which performance drastically worsens (e.g., uUQ with low k). However, for $k > 64$ (MNIST) or $k > 32$ (CIFAR-10), uUQ becomes competitive in accuracy, outdoing other methods’ occupancy ratio (up to around $4\times$ lower). The same considerations hold for regression, in which the uUQ performance boundary is even lower ($k > 2$ for KIBA and $k > 32$ for DAVIS). When $k \leq 64$, uECSQ often exhibits the top performance with uPWS (classification) and uCWS (regression), though usually yielding bigger occupancy than uECSQ. Moreover, uECSQ tend to compress more than uCWS and cPWS.

Summarizing, yet not exhaustively, these experiments suggest to adopt uUQ when enough distinct weights can be used, whereas uECSQ should be employed in the remaining cases, in which uPWS and uCWS (respectively on classification and regression) are valid alternatives.

TABLE III
SUMMARY OF THE PERFORMANCE OF VGG19 TRAINED AND TESTED OVER THE MNIST AND CIFAR-10 DATASETS, AFTER APPLYING DIFFERENT QUANTIZATION TECHNIQUES ON THE DENSE LAYERS. *Perf* MEASURED AS ACCURACY. VALUES IN THE ψ COLUMN REPORT THE RATIO BETWEEN THE HAC COMPRESSED AND UNCOMPRESSED NETWORK SIZES. IN BRACKETS THE ACCURACY OF THE BASELINE.

k	Method	MNIST (0.9954)		CIFAR-10 (0.9344)	
		Perf	ψ	Perf	ψ
2	uCWS	0.2266	0.0313	0.9355	0.0313
	uPWS	0.9951	0.0313	0.9363	0.0313
	uUQ	0.2213	0.0313	0.1981	0.0313
	uECSQ	0.9901	0.0461	0.9368	0.0472
16	uCWS	0.9954	0.1215	0.9366	0.1179
	uPWS	0.9953	0.1212	0.9368	0.1212
	uUQ	0.2159	0.0314	0.1991	0.0316
	uECSQ	0.9957	0.0949	0.9369	0.0801
32	uCWS	0.9957	0.1467	0.9365	0.1513
	uPWS	0.9955	0.1544	0.9365	0.1545
	uUQ	0.2239	0.0322	0.9370	0.0355
	uECSQ	0.9955	0.1338	0.9366	0.1241
64	uCWS	0.9957	0.1835	0.9364	0.1836
	uPWS	0.9955	0.1867	0.9365	0.1867
	uUQ	0.8908	0.0397	0.9362	0.0498
	uECSQ	0.9956	0.1841	0.9366	0.1359
128	uCWS	0.9956	0.2134	0.9364	0.2162
	uPWS	0.9954	0.2184	0.9363	0.2184
	uUQ	0.9955	0.0559	0.9363	0.0736
	uECSQ	0.9958	0.1953	0.9364	0.1787
256	uCWS	0.9957	0.2477	0.9367	0.2468
	uPWS	0.9955	0.2500	0.9363	0.2500
	uUQ	0.9953	0.0971	0.9364	0.1154
	uECSQ	0.9957	0.2283	0.9367	0.2395

Finally, to provide an insight on how pruning interacts with quantization, we repeated the experiments proposing a pruning stage to quantization as done in Sect. V-F, varying p in $\{30, 40, 50, 60, 70, 80, 90, 95, 96, 97, 98, 99\}$, and reporting the top performances (Supplementary Table S5) and the best occupancy configurations ensuring baseline performance (Supplementary Table S6). In terms of best performance, the methods perform similarly (better than the baseline), with uUQ compressing much more than all other methods for classification, substantially confirming the results obtained with no pre-pruning. In terms of best occupancy uECSQ becomes again competitive with uUQ, especially on CIFAR-10 and KIBA. In this setting, even uCWS and uPWS obtain good results (respectively top performance on KIBA and lowest occupancy on DAVIS). On the whole, the tendency shown in Tables III and S4 is confirmed when pruning before sharing weights, with the precious benefit of similarly performing while decreasing the occupancy by almost one order of magnitude.

J. Compressing only convolutional layers

Up to this point only FC layers have been compressed, and in this section we want instead to evaluate the performance of pruning and quantization applied to the convolutional layers of pre-trained models. The aim is obtaining useful information for the final experiment, where both convolutional and FC layers will be compressed simultaneously. Only the performance (accuracy or MSE) is thereby evaluated here, to detect to most meaningful compression configurations on these layers.

TABLE IV
SUMMARY OF THE TESTING PERFORMANCE (ACCURACY FOR VGG19
AND MSE FOR DEEPDTA) OF THE NETWORKS AFTER APPLYING PRUNING
TO CONVOLUTIONAL LAYERS. COLUMN p IS THE LEVEL OF PRUNING.

p	VGG19		DeepDTA	
	MNIST	CIFAR	KIBA	DAVIS
0	0.9954	0.9344	0.1756	0.3223
10	0.9957	0.9355	0.1561	0.2220
20	0.9957	0.9341	0.1565	0.2233
30	0.9957	0.9337	0.1566	0.2238
40	0.9957	0.9333	0.1576	0.2218
50	0.9955	0.9289	0.1571	0.2237
60	0.9956	0.9255	0.1577	0.2224
70	0.9951	0.9179	0.1600	0.2234
80	0.9944	0.9084	0.2223	0.2433
90	0.9917	0.8802	0.3139	0.3492
95	0.9907	0.7950	0.3692	0.4136
96	0.9909	0.7608	0.3796	0.4753
97	0.9903	0.6910	0.4067	0.5180
98	0.9882	0.6154	0.4576	0.5350
99	0.9852	0.5204	0.5446	0.6548

1) *Weight pruning*: here weight pruning has been applied only to the weight tensors of convolutional stages. Results are summarized in Table IV. Pruning helps also in this case, with performance improvements w.r.t. the baseline (row $p = 0$) up to $p = 70$ for MNIST and KIBA, $p = 10$ for CIFAR and $p = 80$ for DAVIS. The top performance achieved are slightly worse than those obtained in Sect. V-F; notwithstanding, it is not possible to achieve the same pruning percentile used on FC layers, which is quite expected, since convolutional layers are responsible for input scan and elaboration. Hence, pruning on these layers cannot always be increased till levels making beneficial the use of sHAC, without having a sensible performance loss. Further, with no more than 10% of pruning (CIFAR-10), even HAC would compress less, while increasing the dot procedure time (see Fig. 1). Finally, this deterioration would also be amplified by the application of weight sharing, still fostering a reduction of pruning percentile. In such a setting, the adoption of our storage formats should be based on the maximum levels of pruning applicable without having an excessive performance loss, as discussed also here below.

2) *Quantization via weight sharing*: the convolutional blocks have been compressed via the four quantization methods compared so far. The unified variant (cfr. Sect. V-H) is considered, sharing weights and dictionaries globally across layers. The results for $k \in \{32, 64, 128, 256\}$ are shown in Table S7, where too low values for k have not been reported because they showed poor results. For classification, quantizing convolutional layers clearly leads to less effective models: indeed, the baseline is almost never improved. Moreover, the difficulty of uUQ with low values of k observed in Sect. V-I is confirmed and intensified, with even uPWS showing a similar behavior for $k = 32$ and 64, corroborating the suspicion that the NN is more sensitive to variations in its convolutional layers. On the other hand, uCWS and uECSQ tend to perform better than the other two techniques, exhibiting higher robustness for small values of k . The results for regression are more stable, as here the tendency is similar to that observed on FC layers: uUQ and uPWS are again competitive with the other two methods, with uUQ achieving the lowest MSE on

KIBA and even when using the smallest k tested. In general, performance is slightly worse and more unstable than that obtained by pruning the same layers, mainly for lower values of k . This suggests to apply not too radical quantizations, and if possible using pruning instead of quantization on convolutional layers. However, low pruning percentages are not enough to fully exploit HAC and sHAC, as well as CSC; thus, for compressing these layers in the experiments of next section, we decided to apply quantization without pruning (to not amplify the above-mentioned instability) and to employ index map representation to compress the obtained tensors. In fact, with low pruning rates, this method showed the best trade-off between compression and dot product time (Sect. V-G).

K. Compressing dense and convolutional layers

In this section we present the more general experiment, aiming at compressing and storing in space-conscious formats all layers of a NN. The results of Sect. V-J suggested to apply low levels of pruning and quantization to convolutional layers, making the index map more suitable to store such layers. In this setting, it is more convenient to not apply pruning, since it helps preventing further accuracy decay, and it does not reduce the occupancy ratio. Therefore, an hybrid format is used in this experiment: index map for convolutional layers, and HAC or sHAC for FC layers, which undergo both pruning and quantization. It is worth nothing that extending the quantization via WS to all layers means, in the unified setup, that convolutional and FC layers will share the same representatives; this experiment offers thereby also a full insight of how the proposed strategies interact and perform when globally applied to the network. In accordance to the results obtained in Sects V-F and V-J2, the values $k \in \{32, 64, 128, 256\}$ have been tested. On the other side, to prune FC layers, the results obtained in Sect. V-F suggested to adopt different values for p on each dataset: $p \in \{90, 92, 95, 97, 99\}$ for MNIST and CIFAR-10, $p \in \{50, 55, 60, 65, 70\}$ for KIBA, and $p \in \{70, 75, 80, 85, 90\}$ for DAVIS.

Finally, the matrices of FC layers have been stored with HAC when it was more convenient than sHAC and this is marked in Supplementary Tables S8–S11 using * besides the corresponding values. To better understand these results, we remark that occupancy ratios reported in the previous sections were limited to FC layers, not to the whole net; hence, since for the index map method the occupancy ratio cannot be lower than 0.25 (even larger when $k > 256$), the overall occupancy ratio is destined to increase with reference to that of FC layers. As a confirmation, the lowest occupancy registered is 0.0486 (uPWS, DAVIS, $k=32$). Further, on VGG19 (the model with larger convolutional block) occupancy ratios are in average higher than on DeepDTA. A first important observation is that performance tends to deteriorate in this setting (as expected), mainly on classification, compared with those obtained when compressing solely convolutional or FC layers. Nevertheless, the top performance achieved is still higher than the baseline on MNIST (uCWS, $p = 92$, $k = 256$) and occupying only the 16.666% of the original network, whereas on CIFAR-10 data the best accuracy is only the 0.14% smaller than the

baseline (uUQ, $p = 95$, $k = 256$), while occupying just the 14.2%. Besides, the occupancy on MNIST can be halved to the detriment of 0.19% of accuracy (uPWS, $p = 97$, $k = 32$). The results with regression are more stable, confirming the trend shown in previous sections. On KIBA, the top performance improves the baseline by 6% with an occupancy of 0.1320 (uCWS, $p = 50$, $k = 64$), and it can compress up to 0.0806, still outperforming the uncompressed model (uUQ, $p = 60$, $k = 32$). On DAVIS, most configurations improve the baseline MSE, among which the best occupancy is 0.0544 (uUQ, $p = 90$, $k = 32$), which means around $20\times$ smaller than the original NN. These results are quite impressive if we consider that model structure has not been modified. Concerning quantization, the results support most of the analyses done so far, with uPWS and uUQ sometimes showing unstable performance for low values of k on classification, uUQ (and sometimes uPWS) often exhibiting the best compression, and uCWS or uECSQ being good compromises between accuracy and space.

Summing up, on all models and data our format can reduce more than $5\times$ the pre-trained NN size, with peaks of around $20\times$, often improving or nearly matching its performance. The higher variability of results observed on some configurations likely depends on the fact that the actual number of clusters k can be smaller than the reported one, due to a potential centroid overlapping during retraining (see Sect. III-C).

VI. CONCLUSIONS

This work proposed two *structure-preserving* CNN representations, HAC and sHAC, to compress pre-trained models while substantially maintaining their accuracy. As they exploit weight pruning and quantization, an extended comparison of four quantization methods based on WS, namely CWS, PWS, UQ and ECSQ, has been initially performed, suggesting that UQ is in average preferable when enough k distinct weights are available (that is, quantization is not too drastic), whereas EQCS should be used in the remaining cases, as an alternative to PWS on classification and to CWS on regression problems. Further, on convolutional layers CWS and ECQS are in general more stable with respect to k variations on classification problems. HAC and sHAC exploited the quantized and pruned weight matrices to apply Huffman coding on the resulting source, and storing the resulting bitstring in a compact array format. A dedicated dot procedure has been implemented to supply an efficient matrix multiplication to evaluate the NN. In a comparison with state-of-the-art matrix compression methods, our formats have definitely shown higher compression rates when matrices are quantized and sufficiently sparse, and in some cases even a faster dot product. When applied to four benchmarks and two publicly retrievable pre-trained models, in most cases they preserved or improved performance, while reducing memory requirements up to around $20\times$. The computed occupancy resulted in all cases much smaller than the theoretical upper bound derived here, thus suggesting that more strict bounds can probably be deduced. We found compressing convolutional layers being more critical than the dense ones, which is reasonable considering the different role

they have in the input processing, but preventing to obtain high levels of pruning and quantization. This limited the application of our formats to these layers, thus future studies will be conveyed in this direction, to extend the representation so as to better exploit lower pruning and quantization levels. Moreover, a finer level of parallelism can be introduced in the dot procedure to further speed up computations, by considering the vector of the offsets in the bitstring denoting the beginning of each column of the compressed matrix, and partitioning the columns in chunks assigned to different threads/cores to perform the corresponding dot products. Finally, coding methodologies less sensitive to source statistics, known as *universal lossless source coding* (e.g., the Lempel–Ziv source coding), can be applied to reduce memory requirements, since they exhibit a smaller overhead than Huffman coding.

ACKNOWLEDGEMENTS

This work has been supported by the Italian MUR PRIN project “Multicriteria data structures and algorithms: from compressed to learned indexes, and beyond” (Prot. 2017WR7SHH).

REFERENCES

- [1] A. Krizhevsky, I. Sutskever, and G. E. Hinton, “Imagenet classification with deep convolutional neural networks,” in *Advances in Neural Inf. Process. Syst.*, 2012, pp. 1097–1105.
- [2] K. Simonyan and A. Zisserman, “Very deep convolutional networks for large-scale image recognition,” in *Int. Conf. on Learning Representations*, 2015.
- [3] S. J. Pan and Q. Yang, “A survey on transfer learning,” *IEEE Trans. Knowl. Data Eng.*, vol. 22, no. 10, pp. 1345–1359, 2010.
- [4] P. Ferragina and G. Vinciguerra, “The PGM-index: a fully-dynamic compressed learned index with provable worst-case bounds,” *PVLDB*, vol. 13, no. 8, pp. 1162–1175, 2020.
- [5] M. Sandler *et al.*, “Mobilenetv2: Inverted residuals and linear bottlenecks,” in *Proc. IEEE Conf. on Comput. Vision and Pattern Recognit.*, 2018, pp. 4510–4520.
- [6] L. Deng *et al.*, “Model compression and hardware acceleration for neural networks: A comprehensive survey,” *Proc. of the IEEE*, vol. 108, no. 4, pp. 485–532, 2020.
- [7] Y. Cheng *et al.*, “A survey of model compression and acceleration for deep neural networks,” *arXiv preprint arXiv:1710.09282*, 2017.
- [8] M. Hagiwara, “Removal of hidden units and weights for back propagation networks,” in *Proc. of 1993 Int. Conf. on Neural Net. (IJCNN-93-Nagoya, Japan)*, vol. 1, 1993, pp. 351–354 vol.1.
- [9] A. S. Weigend, D. E. Rumelhart, and B. A. Huberman, “Generalization by weight-elimination with application to forecasting,” in *Proc. of the 1990 Conf. on Advances in Neural Inf. Process. Syst.*, 1990, p. 875–882.
- [10] D. Whitley, T. Starkweather, and C. Bogart, “Genetic algorithms and neural networks: optimizing connections and connectivity,” *Parallel Computing*, vol. 14, no. 3, pp. 347–361, 1990. [Online]. Available: <https://www.sciencedirect.com/science/article/pii/0167819190900860>
- [11] J. Tu, Y. Zhan, and F. Han, “A neural network pruning method optimized with pso algorithm,” in *2010 Second Int. Conf. on Comput. Model. and Simul.*, vol. 3, 2010, pp. 257–259.
- [12] W. Dally. (2015) High-performance hardware for machine learning. [Online]. Available: <https://www.microsoft.com/en-us/research/video/tutorial-high-performance-hardware-for-machine-learning>
- [13] B. Jacob *et al.*, “Quantization and training of neural networks for efficient integer-arithmetic-only inference,” in *Proc. of the IEEE Conf. on Comput. Vision and Pattern Recognition (CVPR)*, June 2018.
- [14] I. Hubara *et al.*, “Quantized neural networks: Training neural networks with low precision weights and activations,” *J. Mach. Learn. Res.*, vol. 18, no. 1, p. 6869–6898, Jan. 2017.
- [15] S. Gupta *et al.*, “Deep learning with limited numerical precision,” in *Proc. of the 32nd Int. Conf. on Mach. Learn.*, ser. ICML’15, vol. 37. JMLR.org, 2015, p. 1737–1746.

- [16] I. Hubara *et al.*, “Binarized neural networks,” in *Advances in Neural Inf. Process. Syst.*, D. Lee, M. Sugiyama, U. Luxburg, I. Guyon, and R. Garnett, Eds., vol. 29. Curran Associates, Inc., 2016. [Online]. Available: <https://proceedings.neurips.cc/paper/2016/file/d8330f857a17c53d217014ee776bfd50-Paper.pdf>
- [17] E. Park, S. Yoo, and P. Vajda, “Value-aware quantization for training and inference of neural networks,” in *Proc. of the Eur. Conf. on Comput. Vision (ECCV)*, September 2018.
- [18] L. Hou, Q. Yao, and J. T. Kwok, “Loss-aware binarization of deep networks,” in *5th Int. Conf. on Learn. Representations, ICLR 2017, Toulon, France, April 24-26, 2017*. OpenReview.net, 2017. [Online]. Available: <https://openreview.net/forum?id=S1oWIN9ll>
- [19] A. Zhou *et al.*, “Incremental network quantization: Towards lossless CNNs with low-precision weights,” in *5th Int. Conf. on Learn. Representations, ICLR 2017, Toulon, France, April 24-26, 2017*. OpenReview.net, 2017. [Online]. Available: <https://openreview.net/forum?id=HyQJ-mclg>
- [20] S. Han, H. Mao, and W. J. Dally, “Deep compression: Compressing deep neural networks with pruning, trained quantization and Huffman coding,” in *ICLR 2016*, 2015, arxiv:1510.00149.
- [21] G. C. Marinò *et al.*, “Compression strategies and space-conscious representations for deep neural networks,” in *2020 25th Int. Conf. on Pattern Recognition (ICPR)*, 2021, pp. 9835–9842.
- [22] G. C. Marinò *et al.*, “Reproducing the sparse Huffman address map compression for deep neural networks,” in *Reproducible Research in Pattern Recognition*. Cham: Springer International Publishing, 2021, pp. 161–166.
- [23] Y. Choi, M. El-Khamy, and J. Lee, “Universal deep neural network compression,” *IEEE J. Sel. Topics Signal Process.*, vol. 14, no. 4, pp. 715–726, 2020.
- [24] A. Gersho and R. M. Gray, *Vector Quantization and Signal Compression*. USA: Kluwer Academic Publishers, 1991.
- [25] J. Xue, J. Li, and Y. Gong, “Restructuring of deep neural network acoustic models with singular value decomposition,” in *Interspeech*, January 2013.
- [26] T. N. Sainath *et al.*, “Low-rank matrix factorization for deep neural network training with high-dimensional output targets,” in *Proc. IEEE Int. Conf. on Acoust., Speech and Signal Proc.*, 2013.
- [27] L. De Lathauwer, “Decompositions of a higher-order tensor in block terms - part i : Lemmas for partitioned matrices,” *SIAM J. on Matrix Analysis and Appl.*, vol. 30, no. 3, pp. 1022–1032, 2008.
- [28] R. Rigamonti *et al.*, “Learning separable filters,” in *2013 IEEE Conf. on Comput. Vision and Pattern Recognition*, 2013, pp. 2754–2761.
- [29] M. Jaderberg, A. Vedaldi, and A. Zisserman, “Speeding up convolutional neural networks with low rank expansions,” *CoRR*, vol. abs/1405.3866, 2014. [Online]. Available: <http://arxiv.org/abs/1405.3866>
- [30] X. Yu *et al.*, “On compressing deep models by low rank and sparse decomposition,” in *Proc. of the IEEE Conf. on Comput. Vision and Pattern Recognition (CVPR)*, July 2017.
- [31] J. Ba and R. Caruana, “Do deep nets really need to be deep?” in *Advances in Neural Inf. Process. Syst.*, vol. 27. Curran Associates, Inc., 2014. [Online]. Available: <https://proceedings.neurips.cc/paper/2014/file/ea8fcd92d59581717e06eb187f10666d-Paper.pdf>
- [32] G. Hinton, O. Vinyals, and J. Dean, “Distilling the knowledge in a neural network,” *arXiv preprint arXiv:1503.02531*, 2015.
- [33] M. Phuog and C. Lampert, “Towards understanding knowledge distillation,” in *Proc. of the 36th Int. Conf. on Mach. Learn.*, vol. 97. PMLR, 09–15 Jun 2019, pp. 5142–5151. [Online]. Available: <http://proceedings.mlr.press/v97/phuog19a.html>
- [34] S. Mirzadeh *et al.*, “Improved knowledge distillation via teacher assistant: Bridging the gap between student and teacher,” *CoRR*, vol. abs/1902.03393, 2019. [Online]. Available: <http://arxiv.org/abs/1902.03393>
- [35] R. Müller, S. Kornblith, and G. E. Hinton, “When does label smoothing help?” in *Advances in Neural Inf. Proc. Syst.*, vol. 32. Curran Associates, Inc., 2019. [Online]. Available: <https://proceedings.neurips.cc/paper/2019/file/f1748d6b0fd9d439f71450117eba2725-Paper.pdf>
- [36] Y. Tian, D. Krishnan, and P. Isola, “Contrastive representation distillation,” in *Int. Conf. on Learn. Representations*, 2020. [Online]. Available: <https://openreview.net/forum?id=SkgpBJrtvS>
- [37] A. Mallya and S. Lazebnik, “Packnet: Adding multiple tasks to a single network by iterative pruning,” in *2018 IEEE Conf. on Comput. Vision and Pattern Recognition, CVPR 2018, Salt Lake City, UT, USA, June 18-22, 2018*. IEEE Computer Society, 2018, pp. 7765–7773. [Online]. Available: http://openaccess.thecvf.com/content_cvpr_2018/html/Mallya_PackNet_Adding_Multiple_CVPR_2018_paper.html
- [38] P. Molchanov, A. Mallya, S. Tyree, I. Frosio, and J. Kautz, “Importance estimation for neural network pruning,” in *IEEE Conference on Computer Vision and Pattern Recognition, CVPR 2019, Long Beach, CA, USA, June 16-20, 2019*. Computer Vision Foundation / IEEE, 2019, pp. 11 264–11 272. [Online]. Available: http://openaccess.thecvf.com/content_CVPR_2019/html/Molchanov_Importance_Estimation_for_Neural_Network_Pruning_CVPR_2019_paper.html
- [39] P. Molchanov *et al.*, “Pruning convolutional neural networks for resource efficient transfer learning,” *CoRR*, vol. abs/1611.06440, 2016. [Online]. Available: <http://arxiv.org/abs/1611.06440>
- [40] Y. LeCun, J. Denker, and S. Solla, “Optimal brain damage,” in *Advances in Neural Inf. Proc. Syst.*, vol. 2. Morgan-Kaufmann, 1990. [Online]. Available: <https://proceedings.neurips.cc/paper/1989/file/6c9882bbac1c7093bd25041881277658-Paper.pdf>
- [41] H.-G. Han and J.-F. Qiao, “A structure optimisation algorithm for feedforward neural network construction,” *Neurocomput.*, vol. 99, pp. 347–357, Jan. 2013. [Online]. Available: <https://doi.org/10.1016/j.neucom.2012.07.023>
- [42] H. Li *et al.*, “Pruning filters for efficient convnets,” *arXiv preprint arXiv:1608.08710*, 2017.
- [43] J.-H. Luo *et al.*, “Thinet: Pruning cnn filters for a thinner net,” *IEEE Trans. Pattern Anal. Mach. Intell.*, vol. 41, no. 10, pp. 2525–2538, 2019.
- [44] Y. He, X. Zhang, and J. Sun, “Channel pruning for accelerating very deep neural networks,” in *2017 IEEE Int. Conf. on Comput. Vision (ICCV)*, 2017, pp. 1398–1406.
- [45] X. He, Z. Zhou, and L. Thiele, “Multi-task zipping via layer-wise neuron sharing,” in *Advances in Neural Inf. Proc. Syst.*, vol. 31. Curran Associates, Inc., 2018. [Online]. Available: <https://proceedings.neurips.cc/paper/2018/file/ad8e88c0f76fa4fc8e5474384142a00a-Paper.pdf>
- [46] M. Tan *et al.*, “Mnasnet: Platform-aware neural architecture search for mobile,” in *2019 IEEE/CVF Conf. on Comput. Vision and Pattern Recognition (CVPR)*. Los Alamitos, CA, USA: IEEE Computer Society, Jun 2019, pp. 2815–2823. [Online]. Available: <https://doi.ieeecomputersociety.org/10.1109/CVPR.2019.00293>
- [47] J. Chauhan *et al.*, “Performance characterization of deep learning models for breathing-based authentication on resource-constrained devices,” *Proc. ACM Interact. Mob. Wearable Ubiquitous Technol.*, vol. 2, no. 4, Dec. 2018. [Online]. Available: <https://doi.org/10.1145/3287036>
- [48] J. B. McQueen, “Some methods of classification and analysis in multivariate observations,” in *Proc. of fifth Barkley symp. on mathematical statist. and probability*, 1967, pp. 281–297.
- [49] M. Courbariaux *et al.*, “Binaryconnect: Training deep neural networks with binary weights during propagations,” in *Advances in Neural Inf. Proc. Syst.* 28, 2015, pp. 3123–3131.
- [50] L. Deng *et al.*, “Gxnor-net: Training deep neural networks with ternary weights and activations without full-precision memory under a unified discretization framework,” *Neural Networks*, vol. 100, pp. 49–58, 2018.
- [51] H. Gish and J. Pierce, “Asymptotically efficient quantizing,” *IEEE Trans. Inf. Theory*, vol. 14, no. 5, pp. 676–683, 1968.
- [52] P. A. Chou, T. Lookabaugh, and R. M. Gray, “Entropy-constrained vector quantization,” *IEEE Trans. Acoust. Speech, Signal Process.*, vol. 37, no. 1, pp. 31–42, 1989.
- [53] Y. Saad, *Iterative Methods for Sparse Linear Systems*, 2nd ed. USA: Society for Industrial and Applied Mathematics, 2003.
- [54] D. A. Huffman, “A method for the construction of minimum-redundancy codes,” *Proc. of the IRE*, vol. 40, no. 9, pp. 1098–1101, 1952.
- [55] C. E. Shannon, “A mathematical theory of communication,” *Bell Syst. Tech. J.*, vol. 27, no. 3, pp. 379–423, 1948.
- [56] Z. Sultana and S. Akter, “A new approach of a memory efficient Huffman tree representation technique,” in *2012 Int. Conf. on Inform. Electron. Vision (ICIEV)*, 2012, pp. 731–736.
- [57] Y. Lecun *et al.*, “Gradient-based learning applied to document recognition,” *Proc. of the IEEE*, vol. 86, no. 11, pp. 2278–2324, 1998.
- [58] A. Krizhevsky, “Learning multiple layers of features from tiny images,” Master’s thesis, University of Toronto, 2009.
- [59] M. I. Davis *et al.*, “Comprehensive analysis of kinase inhibitor selectivity,” *Nature Biotechnology*, vol. 29, pp. 1046–1051, 2011.
- [60] J. Tang *et al.*, “Making sense of large-scale kinase inhibitor bioactivity data sets: A comparative and integrative analysis,” *J. of Chem. Inf. and Model.*, vol. 54, no. 3, pp. 735–743, 2014.
- [61] H. Öztürk *et al.*, “DeepDTA: deep drug–target binding affinity prediction,” *Bioinformatics*, vol. 34, no. 17, pp. i821–i829, 09 2018.
- [62] A. Elgohary *et al.*, “Compressed linear algebra for large-scale machine learning,” *VLDB J.*, vol. 27, no. 5, pp. 719–744, 2018. [Online]. Available: <https://doi.org/10.1007/s00778-017-0478-1>
- [63] D. J. Rose and R. A. Willoughby, Eds., *Sparse Matrices and Their Applications*, New York, NY, USA, 1972.

Supplementary materials for the article: "Compact representations of convolutional neural networks via weight pruning and quantization"

Giosuè Cataldo Marinò, Alessandro Petrini, Dario Malchiodi, Marco Frasca
Università degli Studi di Milano, Milano, Italy

E-mail: giosue.marino@studenti.unimi.it, {alessandro.petrini, dario.malchiodi, marco.frasca}@unimi.it

arXiv:2108.12704v1 [cs.LG] 28 Aug 2021

TABLE S1

TOP TESTING PERFORMANCE ACHIEVED BY COMPRESSION TECHNIQUES. *Type* IS THE COMPRESSION TECHNIQUE, WHILE *Perf* CONTAINS ACCURACY FOR VGG19 AND MSE FOR DEEPDTA (BASELINE IN BRACKETS). ψ IS THE OCCUPANCY RATIO, WHEREAS * DENOTES sHAC REPRESENTATION AS THE LOWEST OCCUPANCY ON THAT SETTING (W.R.T. HAC). IN BOLD THE BEST RESULTS ON EACH COUPLE NET-DATASET.

Net-Dataset	Type	Config	Perf	ψ
VGG19-MNIST (0.9954)	Pr	96	0.9954	0.0800
	CWS	128-32-32	0.9957	0.3210
	PWS	32-32-2	0.9958	0.3090
	Pr/CWS-a	96/128-32-32	0.9956	0.0390*
	Pr/CWS-b	96/128-32-32	0.9956	0.0390*
	Pr/PWS-a	96/32-128-32	0.9956	0.0260*
	Pr/PWS-b	50/32-32-2	0.9958	0.1870
VGG19-CIFAR10 (0.9344)	Pr	60	0.9365	0.8000
	CWS	32-32-2	0.9371	0.3060
	PWS	32-2-32	0.9363	0.0910
	Pr/CWS-a	60/2-2-32	0.9366	0.0880
	Pr/CWS-b	50/32-32-2	0.9370	0.2160
	Pr/PWS-a	60/2-2-32	0.9363	0.0880
	Pr/PWS-b	98/32-2-32	0.9365	0.0120*
DeepDTA-KIBA (0.1756)	Pr	60	0.1599	0.8000
	CWS	128-128-32-2	0.1679	0.3900
	PWS	32-128-128-32	0.1761	0.4250
	Pr/CWS-a	60/32-128-2-32	0.1666	0.1870
	Pr/CWS-b	30/128-128-32-2	0.1644	0.3300
	Pr/PWS-a	60/128-128-128-32	0.1769	0.2070
	Pr/PWS-b	40/32-128-128-32	0.1683	0.2910
DeepDTA-DAVIS (0.3223)	Pr	80	0.2242	0.4000
	CWS	128-2-128-2	0.2320	0.2120
	PWS	128-32-32-32	0.2430	0.3240
	Pr/CWS-a	80/32-128-2-32	0.2341	0.1050
	Pr/CWS-b	40/128-2-128-2	0.2826	0.1910
	Pr/PWS-a	80/128-128-32	0.2302	0.1220
	Pr/PWS-b	60/128-32-32-32	0.2353	0.1600

TABLE S2

BEST OCCUPANCY RATIO ENSURING NO DECAY IN PERFORMANCE W.R.T. THE UNCOMPRESSED MODEL. SAME NOTATIONS AS IN TABLE S1.

Net-Dataset	Type	Config	Perf	Psi
VGG19-MNIST (0.9954)	Pr	97	0.9953	0.0600
	CWS	128-2-32	0.9954	0.1040
	PWS	1024-2-32	0.9955	0.1260
	Pr/CWS-a	96/2-128-2	0.9954	0.0380*
	Pr/CWS-b	96/128-32-32	0.9956	0.0390*
	Pr/PWS-a	96/32-128-32	0.9956	0.0260*
	Pr/PWS-b	97/32-32-2	0.9955	0.0180*
VGG19-CIFAR10 (0.9344)	Pr	99	0.9357	0.0200
	CWS	2-2-32	0.9360	0.0630
	PWS	2-2-32	0.9351	0.0630
	Pr/CWS-a	60/2-2-32	0.9366	0.0880
	Pr/CWS-b	99/32-32-2	0.9358	0.0060*
	Pr/PWS-a	60/2-2-32	0.9363	0.0880
	Pr/PWS-b	99/32-2-32	0.9363	0.0060*
DeepDTA-KIBA (0.1756)	Pr	60	0.1599	0.8000
	CWS	32-32-2-2	0.1723	0.2280
	PWS	32-128-128-32	0.1761	0.4250
	Pr/CWS-a	60/32-2-32-2	0.1739	0.1270
	Pr/CWS-b	60/128-128-32-2	0.1712	0.2220
	Pr/PWS-a	60/128-128-128-32	0.1769	0.2070
	Pr/PWS-b	50/32-128-128-32	0.1702	0.2430
DeepDTA-DAVIS (0.3223)	Pr	90	0.2425	0.2000
	CWS	2-2-2-2	0.2840	0.0630
	PWS	32-32-2-32	0.2567	0.2370
	Pr/CWS-a	80/32-2-2-32	0.2367	0.0790
	Pr/CWS-b	60/128-2-128-2	0.2906	0.1480
	Pr/PWS-a	90/128-32-32-32	0.2671	0.0600*
	Pr/PWS-b	80/32-2-2-32	0.2943	0.0770



Fig. S1. Overall testing performance for compression methods: a) CWS (HAC format), b) PWS (HAC), c) Pr-CWS a (s_{HAC}), d) Pr-PWS a (s_{HAC}), e), f), g) and h) the same a), b), c) and d) methods, but on regression datasets. X-axis report the compression parameters, while Y-axis measures the performance in term of space occupancy, time ratio, and testing performance (from top to bottom).

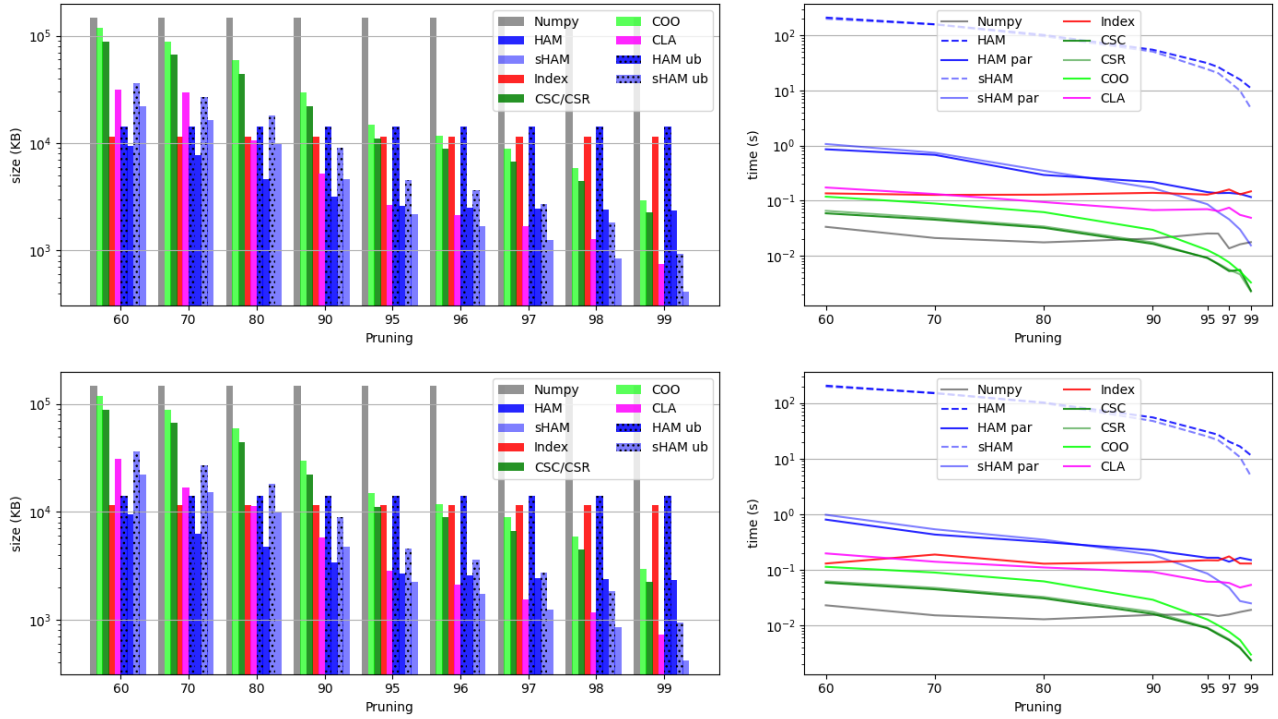


Fig. S2. Average execution times in seconds (graphs on the right) for performing 8 vector matrix product, and memory footprint in KiloBytes (graphs on the left) for storing the compressed representation of the three fully connected layer weight matrices of the VGG19 model. Top rows refer to the model trained on CIFAR10 dataset, bottom row on MNIST dataset. All matrices were subjected to different degrees of pruning and were quantized by weight sharing (CWS) with 32 values. Dotted bars represent the upper bound of sHAM and sHAM sizes evaluated with Corollaries 1 and 2. Times are reported in logarithmic scale.

TABLE S3

COMPARISON BETWEEN UNIFIED QUANTIZATION (ONE k FOR ALL LAYERS) AND NON-UNIFIED QUANTIZATION (DIFFERENT k FOR EACH LAYER). THE CHOSEN CONFIGURATIONS FOR NON-UNIFIED METHODS ARE THOSE REPORTED IN TABLE S2. MODELS MARKED WITH * ARE THOSE WHERE sHAM COMPRESSED MORE. TESTING PERFORMANCE BASELINE IN BRACKETS.

Net-Dataset	Type	Config	Perf	ψ
VGG19-MNIST (0.9954)	CWS	128-2-32	0.9954	0.1040
	uCWS	162	0.9957	0.2265
	uCWS*	16	0.9954	0.1215
	PWS	1024-2-32	0.9955	0.1260
	uPWS	1058	0.9955	0.3121
	uPWS*	2	0.9955	0.0313
VGG19-CIFAR10 (0.9344)	CWS	2-2-32	0.9360	0.0630
	uCWS	36	0.9367	0.1567
	uCWS*	2	0.9362	0.0313
	PWS	2-2-32	0.9351	0.0630
	uPWS	36	0.9364	0.1576
	uPWS*	2	0.9364	0.0313
DeepDTA-KIBA (0.1756)	CWS	32-32-2-2	0.1723	0.2280
	uCWS	68	0.1601	0.1843
	uCWS*	8	0.1661	0.0848
	PWS	32-128-128-32	0.1761	0.4250
	uPWS	320	0.1631	0.2642
	uPWS*	32	0.1718	0.1553
DeepDTA-DAVIS (0.3223)	CWS	2-2-2-2	0.2840	0.0630
	uCWS	8	0.2637	0.0900
	uCWS*	4	0.2751	0.0606
	PWS	32-32-2-32	0.2430	0.2370
	uPWS	98	0.2276	0.2091
	uPWS*	8	0.2783	0.0865

TABLE S4

SUMMARY OF THE PERFORMANCE OF DEEPTA DNN TRAINED AND TESTED OVER THE KIBA AND DAVIS DATASETS, AFTER APPLYING DIFFERENT QUANTIZATION TECHNIQUES ON THE DENSE LAYERS. PERF. MEASURED IN MSE. VALUES IN THE ψ COLUMN REPORT THE RATIO BETWEEN THE HAC COMPRESSED AND UNCOMPRESSED NETWORK SIZES. IN BRACKETS THE BASELINE MSE VALUES.

k	Method	KIBA (0.1756)		DAVIS (0.3223)	
		Perf	ψ	Perf	ψ
2	uCWS	80.0142	0.0313	22.3118	0.0313
	uPWS	0.7699	0.0313	29.6357	0.0313
	uUQ	105.6028	0.0313	22.3100	0.0313
	uECSQ	80.0640	0.0313	22.3111	0.0313
16	uCWS	0.1625	0.1197	0.2321	0.1211
	uPWS	0.1847	0.1225	0.2581	0.1217
	uUQ	0.1696	0.0523	22.3108	0.0413
	uECSQ	0.1631	0.1031	0.2309	0.1059
32	uCWS	0.1606	0.1491	0.2203	0.1502
	uPWS	0.1713	0.1551	0.2432	0.1550
	uUQ	0.1639	0.0841	6.9812	0.0652
	uECSQ	0.1600	0.0933	0.2283	0.1183
64	uCWS	0.1608	0.1825	0.2237	0.1853
	uPWS	0.1674	0.1873	0.2258	0.1873
	uUQ	0.1639	0.1161	0.2244	0.0959
	uECSQ	0.1618	0.1237	0.2251	0.1636
128	uCWS	0.1608	0.2149	0.2214	0.2169
	uPWS	0.1659	0.2194	0.2323	0.2194
	uUQ	0.1620	0.1498	0.2304	0.1272
	uECSQ	0.1615	0.1894	0.2242	0.1967
256	uCWS	0.1600	0.2446	0.2272	0.2494
	uPWS	0.1628	0.2519	0.2228	0.2519
	uUQ	0.1613	0.1772	0.2204	0.1593
	uECSQ	0.1603	0.2187	0.2309	0.2069

TABLE S5

SUMMARY OF THE PRUNING AND QUANTIZATION CONFIGURATIONS YIELDING THE BEST PERFORMING MODEL IN TERMS OF ACCURACY. TESTING PERFORMANCE BASELINE IN BRACKETS.

Net-Dataset	Type	$p-k$	Perf	ψ
VGG19-MNIST (0.9954)	PruCWS	60-16	0.9955	0.0777
	PruPWS	60-32	0.9955	0.0807
	PruUQ*	99-32	0.9954	0.0057
	PruECSQ*	95-16	0.9954	0.0276
VGG19-CIFAR-10 (0.9344)	PruCWS	95-32	0.9365	0.0338
	PruPWS	60-16	0.9366	0.0617
	PruUQ*	99-16	0.9363	0.00567
	PruECSQ	60-16	0.9365	0.07537
DeepDTA-KIBA (0.1756)	PruCWS	60-16	0.1645	0.07907
	PruPWS	60-64	0.1700	0.09017
	PruUQ	60-64	0.1630	0.08247
	PruECSQ	60-32	0.1645	0.0918
DeepDTA-DAVIS (0.3223)	PruCWS	60-16	0.2218	0.0795
	PruPWS	60-64	0.2269	0.0875
	PruUQ	60-64	0.2203	0.0675
	PruECSQ	60-32	0.2199	0.0887

TABLE S6

SUMMARY OF THE PRUNING AND QUANTIZATION CONFIGURATIONS OBTAINING THE BEST PERFORMING MODEL IN TERMS OF COMPRESSION RATIO. TESTING PERFORMANCE BASELINE IN BRACKETS.

Net-Dataset	Type	$p-k$	Perf	ψ
VGG19-MNIST (0.9954)	PruCWS	80-64	0.9954	0.0577
	PruPWS	60-32	0.9954	0.0807
	PruUQ*	99-32	0.9954	0.0057
	PruECSQ*	95-16	0.9954	0.0276
VGG19-CIFAR10 (0.9344)	PruCWS*	99-32	0.9361	0.0055
	PruPWS*	99-32	0.9344	0.0055
	PruUQ*	99-16	0.9363	0.0056
	PruECSQ*	99-32	0.9363	0.0055
DeepDTA-KIBA (0.1756)	PruCWS	60-16	0.1645	0.0790
	PruPWS	60-64	0.1700	0.0901
	PruUQ	60-16	0.1698	0.0596
	PruECSQ	60-16	0.1660	0.0766
DeepDTA-DAVIS (0.3223)	PruCWS*	95-64	0.3037	0.0268
	PruPWS*	97-32	0.3187	0.0159
	PruUQ	90-16	0.2383	0.0365
	PruECSQ*	95-32	0.3127	0.0271

TABLE S7

PERFORMANCE ACHIEVED AFTER APPLYING QUANTIZATION VIA WEIGHT SHARING TECHNIQUES ONLY TO CNN LAYERS. FOR DEEPTA, PERFORMANCE IS MEASURED AS MSE; FOR VGG19, AS ACCURACY (BASELINE IN BRACKETS).

k	Method	VGG19		DeepDTA	
		MNIST (0.9954)	CIFAR-10 (0.9344)	KIBA (0.1756)	DAVIS (0.3223)
32	uCWS	0.9941	0.9109	0.1570	0.2221
	uPWS	0.9918	0.1129	0.1634	0.2209
	uUQ	0.1434	0.1210	0.1557	0.2234
	uECSQ	0.9943	0.8941	0.1582	0.2301
64	uCWS	0.9943	0.9036	0.1575	0.2219
	uPWS	0.9932	0.1234	0.1602	0.2234
	uUQ	0.2059	0.1746	0.1571	0.2214
	uECSQ	0.9933	0.9013	0.1586	0.2326
128	uCWS	0.9943	0.9133	0.1563	0.2189
	uPWS	0.9934	0.9020	0.1579	0.2211
	uUQ	0.2076	0.1842	0.1568	0.2216
	uECSQ	0.9952	0.9030	0.1582	0.2315
256	uCWS	0.9946	0.9196	0.1563	0.2193
	uPWS	0.9936	0.9065	0.1571	0.2191
	uUQ	0.2106	0.9336	0.1576	0.2189
	uECSQ	0.9955	0.9073	0.1581	0.2204

TABLE S8
 SUMMARY OF THE RESULTS OF THE APPLICATION OF PRUNING AND QUANTIZATION APPLIED TO DENSE LAYERS AND QUANTIZATION ON CONVOLUTIONAL LAYERS OF VGG19 TRAINED ON THE MNIST DATASET. PERFORMANCE IS REPORTED AS ACCURACY; COMPRESSION RATIO (ψ) IN BRACKETS. BASELINE OF THE UNCOMPRESSED MODEL REPORTED IN BOLD. MODELS COMPRESSED WITH sHACARE MARKED WITH A STAR (*), OTHERWISE HACWAS USED.

VGG19 - MNIST (0.9954)						
k (CNN and Dense)	Method	PR Dense: 90	PR Dense: 92	PR Dense: 95	PR Dense: 97	PR Dense: 99
32	uCWS	0.9936 (0.1150)	0.9937 (0.1144)	0.9936 (0.1103*)	0.9916 (0.1047*)	0.9937 (0.0992*)
	uPWS	0.1538 (0.0988)	0.9935 (0.0981)	0.9934 (0.0940*)	0.9935 (0.0884*)	0.9932 (0.0831*)
	uUQ	0.2258 (0.1131)	0.1374 (0.1128)	0.1945 (0.1087*)	0.1898 (0.1038*)	0.1135 (0.0989*)
	uECSQ	0.9931 (0.1167)	0.994 (0.1154)	0.9945 (0.1107*)	0.9944 (0.1048*)	0.9929 (0.0992*)
64	uCWS	0.9943 (0.1338)	0.9941 (0.1323)	0.9914 (0.1272*)	0.9932 (0.1211*)	0.9943 (0.1153*)
	uPWS	0.9938 (0.1162)	0.9942 (0.1150)	0.9943 (0.1105*)	0.9943 (0.1047*)	0.9942 (0.0992*)
	uUQ	0.1325 (0.1292)	0.1334 (0.1289)	0.1361 (0.1254*)	0.1330 (0.1203*)	0.1221 (0.1152*)
	uECSQ	0.9941 (0.1344)	0.9942 (0.1328)	0.9465 (0.1275*)	0.9948 (0.1213*)	0.9938 (0.1154*)
128	uCWS	0.9944 (0.1509)	0.9941 (0.1492)	0.9952 (0.1438*)	0.9931 (0.1377*)	0.9941 (0.1316*)
	uPWS	0.9937 (0.1336)	0.9935 (0.1322)	0.9939 (0.1271*)	0.9796 (0.1211*)	0.9592 (0.1153*)
	uUQ	0.2090 (0.1302)	0.1887 (0.1294)	0.1661 (0.1257*)	0.1601 (0.1204*)	0.2007 (0.1152*)
	uECSQ	0.9946 (0.1520)	0.9949 (0.1501)	0.9925 (0.1442*)	0.9926 (0.1378*)	0.9943 (0.1316*)
256	uCWS	0.9945 (0.1685)	0.9955 (0.1666)	0.9952 (0.1608*)	0.9953 (0.1540*)	0.9947 (0.1472*)
	uPWS	0.9940 (0.1512)	0.9939 (0.1494)	0.9867 (0.1438*)	0.9945 (0.1375*)	0.9886 (0.1315*)
	uUQ	0.1247 (0.1463)	0.1170 (0.1459)	0.1993 (0.1423*)	0.1139 (0.1368*)	0.2077 (0.1313*)
	uECSQ	0.9949 (0.1696)	0.9952 (0.1674)	0.9953 (0.1611*)	0.9948 (0.1543*)	0.9938 (0.1478*)

TABLE S9
 SUMMARY OF THE RESULTS OF THE APPLICATION OF PRUNING AND QUANTIZATION APPLIED TO DENSE LAYERS AND QUANTIZATION ON CONVOLUTIONAL LAYERS OF VGG19 TRAINED ON THE CIFAR10 DATASET. PERFORMANCE IS REPORTED AS ACCURACY; COMPRESSION RATIO (ψ) IN BRACKETS. BASELINE OF THE UNCOMPRESSED MODEL REPORTED IN BOLD. MODELS COMPRESSED WITH sHAC ARE MARKED WITH A STAR (*), OTHERWISE HAC WAS USED.

VGG19 - CIFAR10 (0.9344)						
k (CNN and Dense)	Method	PR Dense: 90	PR Dense: 92	PR Dense: 95	PR Dense: 97	PR Dense: 99
32	uCWS	0.8810 (0.1161)	0.8818 (0.1150)	0.8655 (0.1104*)	0.8668 (0.1047*)	0.8822 (0.0992*)
	uPWS	0.1173 (0.0993)	0.1170 (0.0983)	0.1233 (0.0941*)	0.1221 (0.0886*)	0.1133 (0.0831*)
	uUQ	0.1335 (0.1131)	0.1110 (0.1128)	0.1061 (0.1087*)	0.1362 (0.1038*)	0.1180 (0.0989*)
	uECSQ	0.8706 (0.1172)	0.8731 (0.1176)	0.8731 (0.1139)	0.8668 (0.1049*)	0.8794 (0.0992*)
64	uCWS	0.8898 (0.1341)	0.8904 (0.1328)	0.8892 (0.1274*)	0.8913 (0.1213*)	0.8923 (0.1154*)
	uPWS	0.1210 (0.1165)	0.1216 (0.1153)	0.1158 (0.1105*)	0.1156 (0.1048*)	0.1098 (0.0992*)
	uUQ	0.1385 (0.1292)	0.1601 (0.1289)	0.1659 (0.1255*)	0.1673 (0.1203*)	0.1678 (0.1152*)
	uECSQ	0.8822 (0.1348)	0.8774 (0.1331)	0.8799 (0.1307)	0.8799 (0.1214*)	0.8757 (0.1154*)
128	uCWS	0.8919 (0.1514)	0.8944 (0.1497)	0.8936 (0.1441*)	0.9022 (0.1376*)	0.9027 (0.1315*)
	uPWS	0.1210 (0.1339)	0.1164 (0.1324)	0.1290 (0.1272*)	0.1172 (0.1212*)	0.1263 (0.1154*)
	uUQ	0.1440 (0.1297)	0.1409 (0.1294)	0.1414 (0.1258*)	0.1494 (0.1206*)	0.1323 (0.1152*)
	uECSQ	0.8917 (0.1523)	0.8889 (0.1503)	0.8899 (0.1475)	0.8955 (0.1379*)	0.8995 (0.1316*)
256	uCWS	0.9083 (0.1693)	0.9089 (0.1672)	0.9089 (0.1611*)	0.9088 (0.1544*)	0.9080 (0.1478*)
	uPWS	0.1270 (0.1515)	0.1239 (0.1497)	0.1207 (0.1440*)	0.1244 (0.1377*)	0.1335 (0.1315*)
	uUQ	0.9317 (0.1461)	0.9305 (0.1457)	0.9331 (0.1420*)	0.9328 (0.1367*)	0.9309 (0.1314*)
	uECSQ	0.9034 (0.1699)	0.9040 (0.1676)	0.9031 (0.1643)	0.9052 (0.1544*)	0.9037 (0.1478*)

TABLE S10

SUMMARY OF THE RESULTS OF THE APPLICATION OF PRUNING AND QUANTIZATION APPLIED TO DENSE LAYERS AND QUANTIZATION ON CONVOLUTIONAL LAYERS OF DEEPTA TRAINED ON THE KIBA DATASET. PERFORMANCE IS REPORTED AS MSE; COMPRESSION RATIO (ψ) IN BRACKETS. BASELINE OF THE UNCOMPRESSED MODEL REPORTED IN BOLD.

DeepDTA - KIBA (0.1756)						
k (CNN and Dense)	Method	PR Dense: 50	PR Dense: 55	PR Dense: 60	PR Dense: 65	PR Dense: 70
32	uCWS	0.1680	0.1693	0.1717	0.1780	0.1954
		(0.1149)	(0.1085)	(0.1015)	(0.0953)	(0.0884)
	uPWS	0.1918	0.1978	0.1908	0.3108	0.3946
		(0.1021)	(0.0950)	(0.0883)	(0.0779)	(0.0712)
	uUQ	0.1686	0.1690	0.1732	0.1987	0.3272
(0.0869)	(0.0839)	(0.0806)	(0.0773)	(0.0733)		
64	uCWS	0.1649	0.1664	0.1704	0.1758	0.1938
		(0.1320)	(0.1240)	(0.1158)	(0.1088)	(0.1007)
	uPWS	0.1781	0.1789	0.1827	0.1956	0.3533
		(0.1198)	(0.1115)	(0.1032)	(0.0913)	(0.0833)
	uUQ	0.1658	0.1674	0.1742	0.1906	0.1985
(0.1040)	(0.0987)	(0.9418)	(0.0897)	(0.0848)		
128	uCWS	0.1657	0.1670	0.1702	0.1769	0.4429
		(0.1514)	(0.1419)	(0.1323)	(0.1229)	(0.1141)
	uPWS	0.1734	0.1741	0.1735	0.1876	0.2804
		(0.1377)	(0.1278)	(0.1144)	(0.1050)	(0.0956)
	uUQ	0.1652	0.1670	0.1734	0.1866	0.1946
(0.1218)	(0.1162)	(0.1097)	(0.1036)	(0.0974)		
uECSQ	0.1649	0.1678	0.1707	0.4311	0.4977	
(0.1546)	(0.1463)	(0.1353)	(0.1257)	(0.1148)		
256	uCWS	0.1652	0.1669	0.1705	0.4485	0.4111
		(0.1690)	(0.1585)	(0.1480)	(0.1371)	(0.1264)
	uPWS	0.1720	0.1737	0.1762	0.3684	0.4418
		(0.1555)	(0.1441)	(0.1294)	(0.1186)	(0.1078)
	uUQ	0.1654	0.1662	0.1706	0.1766	0.1947
(0.1409)	(0.1333)	(0.1259)	(0.1183)	(0.1103)		
uECSQ	0.1659	0.1673	0.1714	0.4221	0.5349	
(0.1651)	(0.1557)	(0.1453)	(0.1312)	(0.1202)		

TABLE S11
 SUMMARY OF THE RESULTS OF THE APPLICATION OF PRUNING AND QUANTIZATION APPLIED TO DENSE LAYERS AND QUANTIZATION ON CONVOLUTIONAL LAYERS OF DEEPTA TRAINED ON THE DAVIS DATASET. PERFORMANCE IS REPORTED AS MSE; COMPRESSION RATIO (ψ) IN BRACKETS. BASELINE OF THE UNCOMPRESSED MODEL REPORTED IN BOLD.

DeepDTA - DAVIS (0.3223)						
k (CNN and Dense)	Method	PR Dense: 70	PR Dense: 75	PR Dense: 80	PR Dense: 85	PR Dense: 90
32	uCWS	0.2309	0.2342	0.2408	0.2544	0.2530
		(0.0866)	(0.0789)	(0.0733)	(0.0666)	(0.0607)
	uPWS	0.4050	0.3990	0.4180	0.3626	0.5045
		(0.0702)	(0.0642)	(0.0584)	(0.0528)	(0.0486)
	uUQ	0.2331	0.2376	0.2397	0.2482	0.2801
(0.0644)	(0.0633)	(0.0603)	(0.0575)	(0.0544)		
64	uCWS	0.2310	0.2402	0.2441	0.2441	0.2552
		(0.0901)	(0.0771)	(0.0712)	(0.0634)	(0.0564)
	uPWS	0.2386	0.2346	0.2372	0.2524	0.2603
		(0.0995)	(0.0920)	(0.0844)	(0.0663)	(0.0590)
	uUQ	0.2539	0.2552	0.2610	0.2842	0.3271
(0.0825)		(0.0747)	(0.0679)	(0.061)	(0.0549)	
uECSQ	0.2344	0.2369	0.2410	0.2525	0.2584	
(0.0748)	(0.0719)	(0.0685)	(0.0645)	(0.0597)		
128	uCWS	0.2364	0.2348	0.2356	0.2414	0.2467
		(0.0949)	(0.0866)	(0.0805)	(0.0714)	(0.0632)
	uPWS	0.2311	0.2301	0.2440	0.2412	0.2525
		(0.1114)	(0.1026)	(0.0791)	(0.0705)	(0.0598)
	uUQ	0.2535	0.2474	0.2538	0.2637	0.2755
(0.0949)		(0.0857)	(0.0772)	(0.0690)	(0.0576)	
uECSQ	0.2295	0.2305	0.2342	0.2423	0.2636	
(0.0860)	(0.0818)	(0.0763)	(0.0716)	(0.0667)		
256	uCWS	0.2343	0.2335	0.2355	0.2377	0.2570
		(0.1031)	(0.0934)	(0.0898)	(0.0794)	(0.0698)
	uPWS	0.2267	0.2273	0.2346	0.2411	0.2718
		(0.1252)	(0.1145)	(0.0862)	(0.0770)	(0.0644)
	uUQ	0.2397	0.2390	0.2440	0.2460	0.2581
(0.1071)		(0.0965)	(0.0865)	(0.0770)	(0.0642)	
uECSQ	0.2305	0.2391	0.2393	0.2419	0.2505	
(0.0943)	(0.0882)	(0.0822)	(0.0760)	(0.0698)		
256	uCWS	0.2291	0.2286	0.2329	0.2419	0.2663
		(0.1103)	(0.1020)	(0.0995)	(0.0876)	(0.0765)
	uPWS	0.2397	0.2390	0.2440	0.2460	0.2581
		(0.1071)	(0.0965)	(0.0865)	(0.0770)	(0.0642)
	uUQ	0.2305	0.2391	0.2393	0.2419	0.2505
(0.0943)		(0.0882)	(0.0822)	(0.0760)	(0.0698)	
uECSQ	0.2291	0.2286	0.2329	0.2419	0.2663	
(0.1103)	(0.1020)	(0.0995)	(0.0876)	(0.0765)		